UNIVERSITY OF LEEDS

This is a repository copy of *The nature, origin and significance of luminescent layers in the Bazhenov Shale Formation of West Siberia, Russia*.

White Rose Research Online URL for this paper:
http://eprints.whiterose.ac.uk/140787/

Version: Accepted Version

Article:
Shaldybin, MV, Wilson, MJ, Wilson, L et al. (13 more authors) (2019) The nature, origin and significance of luminescent layers in the Bazhenov Shale Formation of West Siberia, Russia. Marine and Petroleum Geology, 100. pp. 358-375. ISSN 0264-8172

https://doi.org/10.1016/j.marpetgeo.2018.11.022

© 2018 Elsevier Ltd. All rights reserved. Licensed under the Creative Commons Attribution-Non Commercial No Derivatives 4.0 International License (https://creativecommons.org/licenses/by-nc-nd/4.0/).

Reuse
This article is distributed under the terms of the Creative Commons Attribution-NonCommercial-NoDerivs (CC BY-NC-ND) licence. This licence only allows you to download this work and share it with others as long as you credit the authors, but you can't change the article in any way or use it commercially. More information and the full terms of the licence here: https://creativecommons.org/licenses/

Takedown
If you consider content in White Rose Research Online to be in breach of UK law, please notify us by emailing eprints@whiterose.ac.uk including the URL of the record and the reason for the withdrawal request.

White Rose university consortium
Universities of Leeds, Sheffield & York

eprints@whiterose.ac.uk
https://eprints.whiterose.ac.uk/

Graphical Abstract

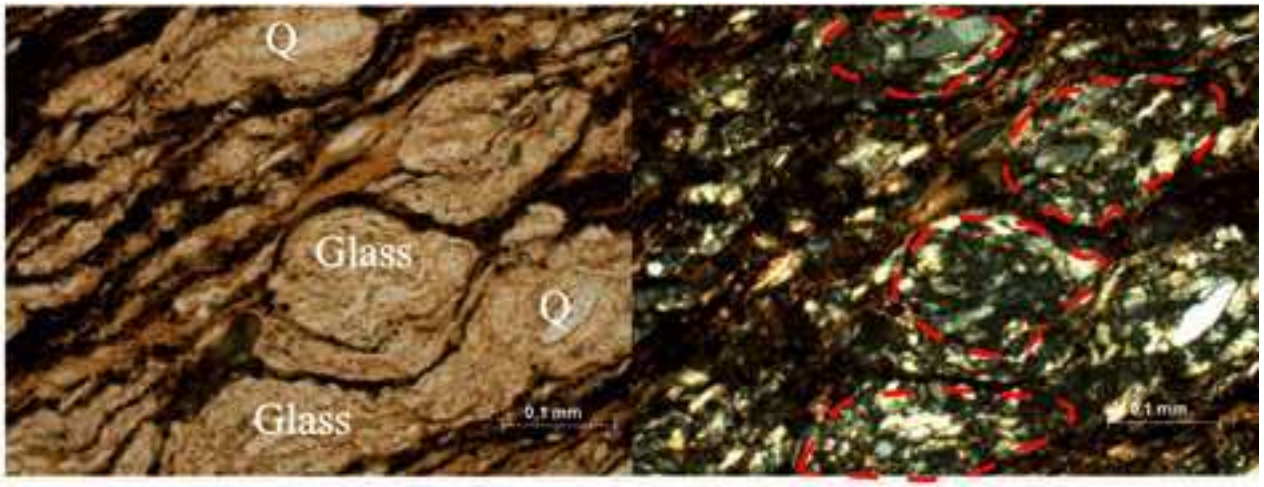

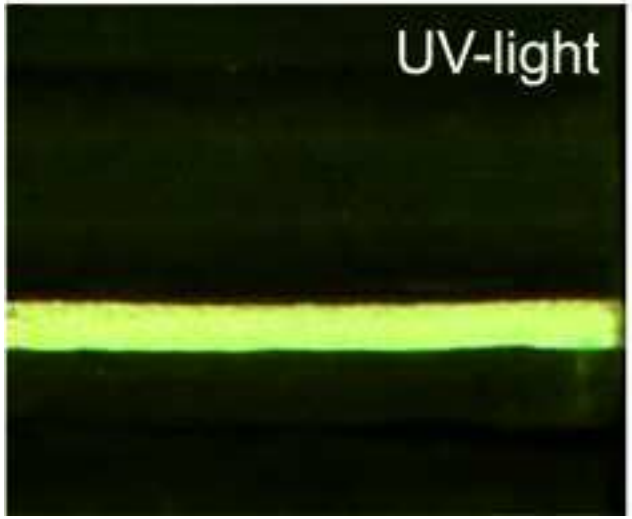

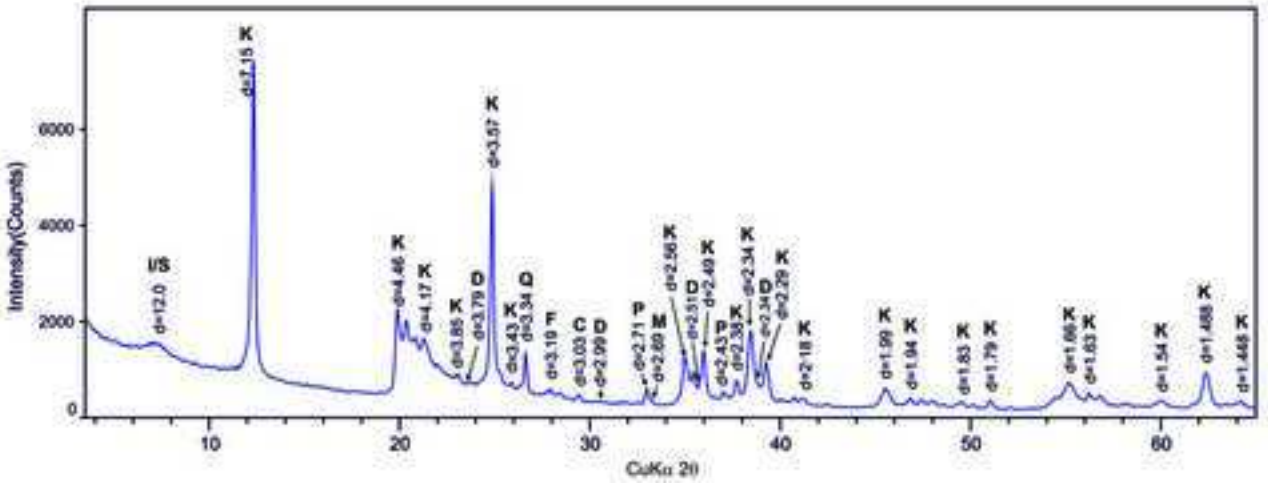

*Revised Manuscript (clean copy)
Click here to view linked References

The Nature, Origin and Significance of Luminescent Layers in the Bazhenov Shale Formation of West Siberia, Russia

[1]Shaldybin, M.V., [1,2]Wilson, M.J., [2]Wilson, L., [3]Lopushnyak, Yu.M., [4]Brydson, R., [5,6]Krupskaya, V.V., [1]Deeva, E.S., [3]Glotov, A.V., [1]Goncharov, I.V., [1]Samoilenko, V.V., [1]Arbuzov, S.I., [3]Bether, O.V., [2]Fraser, A.R., [7]Bowen, L., [2]White, D., [1]Dorofeeva N.V.

[1]Tomsk Polytechnic University, Russia; [2]James Hutton Institute, UK; [3]Tomsk State University, Russia; [4]School of Chemical and Process Engineering, University of Leeds, UK; [5]Institute of Geology of Ore Deposits, Petrography, Mineralogy and Geochemistry Russian Academy of Science (IGEM RAS), Russia, [6]Lomonosov Moscow State University, Russia, [7]Department of Physics, Durham University, Durham, UK

Abstract

Argillites that strongly luminesce under UV radiation were detected in the Bazhenov Shale Formation (BSF) of the West Siberian Basin during routine core examination and found to be persistent over a wide lateral area. The mineralogy and fabric of these luminescent layers were characterized by optical and fluorescence microscopy, SEM, TEM, XRD and IR methods. Optical and fluorescence microscopy showed that the luminescent layers were to a large extent derived from volcanic ash falls and could be described as meta-tuffites, although normal detrital sedimentation continued at the same time. The layers have a thickness of several mm to a maximum of 3-4cm and can be defined as a clay-rich regional horizons. XRD showed that two principal clay minerals were present, namely a kaolinite, possibly with some dickite stacking, (kaolin-rich) and a mixed-layer illite-smectite (I/S) with R1 to R2 ordering similar to that found in K-bentonite. Total organic matter in the luminescent layers is much lower than that in the enclosing BSF clayey-silty siliceous sediments above and below as shown by pyrolytic analyses. Evidence is presented that the luminescent characteristic of the argillites is related to their clay mineralogy, specifically to their content

of kaolin minerals, although a contribution from nitrogenous organic matter cannot be entirely discounted. In some ways the luminescent argillites can be compared with bentonites associated with ash transformations or with tonsteins in coal beds, which are also derived from volcanic ash falls and contain highly crystalline kaolinite. However, tonsteins originate at or near land surface whereas the argillites were apparently formed in the deep ocean. But just as tonsteins can be used for detailed stratigraphic studies and are valuable in the context of coal exploration, so may the luminescent argillites prove to be significant both stratigraphically and in the search for economic hydrocarbon deposits, bearing in mind that their clay mineralogy may be sensitive to temperature and depth of burial and related to their placement in the oil and gas window.

KEYWORDS. Bazhenov Shale, Luminescent Layers, Kaolinite, Dickite, Illite-Smectite, Tonsteins, K-bentonite

1. Introduction

The Bazhenov Shale Formation (BSF) occurs over a million square km in west Siberia and is widely accepted as having acted as the principal source for the hydrocarbon resources of the West Siberian Basin (Ulmishek, 2003). This basin formed a huge sedimentary depocentre extending from the southern part of west Siberia northwards to the Kara Sea (Fig. 3) during Mesozoic to Cenozoic times, and overlies a basement complex of tectonically altered, metamorphosed rocks of Palaeozoic age which formed part of the Pangea super continent. The BSF is of Upper Jurassic (Volgian) age and its detailed composition and genesis has been studied by many Russian researchers from 1960 onwards and more recently by Kontorovich et al. (1998), Zanin et al. (1999), Eder et al. (2003) and Zanin et al. (2003). The mineralogy and geochemistry of the BSF were characterized by Zanin et al. (2008) who concluded that it was made up of three main rock types, namely (a) clayey-silty siliceous

rocks and cherts containing high organic matter and dark-brown in color, (b) argillites, where the clay content exceeds 40% containing low organic matter and of a lighter brown color (Fig. 1) and (c) rocks described as "anomalous" and which could be of a clayey, silty or sandy nature. Argillites are frequently found inter-bedded with the clayey-silty siliceous rocks (Zanin et al., 2008). Dolomitic rocks also occur sporadically within the BSF sequence. Based on mineralogical and chemical criteria the depositional environment of the most widely occurring clayey-siliceous rocks is thought to have been characterized by extremely reducing anoxic conditions, while the argillites are considered to represent distal turbidites that were deposited in dysoxic to suboxic conditions. The anomalous clayey, silty, sandy rocks were considered to have been deposited in channels under oxic conditions.

The present study was prompted by the observation during routine core examination of the BSF highly luminescent under UV light occurred at certain points in the sequence of siliceous silty shales that make up the majority of the BSF (Fig. 2). These luminescent layers appear to be so laterally extensive that they could possibly be of use as stratigraphic markers. Clearly, however, these layers require to be investigated in detail with regard to their nature and origin if their value in correlation studies as well as in other issues is to be established with confidence. The objective of the present paper, therefore, is to characterize the mineralogical and chemical nature of these luminescent layers, to determine the likely origin of the luminescence of these layers, and to assess whether there is a rational basis for the possible use of these layers as stratigraphic markers in the BSF as a whole.

2. Materials

2.1. Geological Setting

The BSF is usually 20 to 40 m in thickness, although in certain localities thicknesses of up to 60 m have been recorded. The shales are black or dark-brown in colour and are high in

organic matter, with total content of C_{org} in the range of 2 to >11% with an average of 4%. The chemical composition of the organic matter corresponds to kerogen type II (Goncharov et al., 2014). This indicates a high potential for hydrocarbon occurrence that could be explored for oil and gas. The essentially detrital nature of the Bazhenov Shales is evident from thin sections, although the role of diagenesis as a determinant of the overall shale mineralogy is also important as shown by Shaldybin et al. (2017).

Sedimentation rates for the clayey-silty siliceous rocks of the BSF are thought to have been extremely low especially within the deepest parts of the sedimentary basin. Thus, Zanin et al. (2008) calculated a rate of 0.4 to 0.5 cm per 1000 years on the basis of the average thickness of the BSF and the time during which the formation was deposited, a rate generally consistent with bioclastic sedimentation in deep water environments (Einsele, 2000; Jenkyns and Clayton, 1986). Sedimentation rates for the argillites, are considered to have been very much faster, bearing in mind their origin as distal turbidites.

The BSF is thought to have originated in an isolated, marine basin analogous to the Black Sea where reducing conditions and intensive hydrogen sulfide generation preserved abundant organic matter (Vyssotski et al., 2006). The salinity of the Bazhenov Sea as determined by the B/Ga ratios corresponded to normal marine conditions for clayey-silty silceous rocks and a more brackish environment for the argillites (Zanin et al., 2008). However, there have been a variety of opinions concerning the depth of the Bazhenov Sea (Zanin et al., 2008 and references therein). Early studies favoured a shallow depth (~10 m) but this was not supported by later research which pointed to much greater palaeo-water depths. Thus, Vyssotski et al. (2006) suggested that at certain stages of development the Bazhenov Sea was 1200 m deep in its central part, although Zanin et al. (2008) conclude that optimum depths of 500 m or deeper are more likely. Beginning in the Upper Oxfordian, the sediment of the

Bazhenov Sea is thought to have been deposited over a period of 8 to 10 million years. This deep-water basin was gradually filled in Neocomian times by a succession of deltaic clastic wedges (clinoforms) prograding towards the west and derived from erosion of the Siberian platform (Ulmishek, 2003). Shallow marine sedimentation, largely of siliciclastic material, continued during Lower Cretaceous times, building up to a thickness of 1.4 to 1.5 km. With continuing sedimentation the total thickness of the Cretaceous and Cenozoic sediments overlying the BSF approaches 2.75 km.

2.2. Sampling

Core samples of were obtained from 10 wells within the Bazhenov Shale Formation. Figure 3 shows the area covered by these wells, extending for 500km from east to west and 400km from north to south. Samples were obtained from cores taken at depths 2200 to 2450 meters that represent the organic-rich Bazhenov Shale. Investigations were concentrated on the luminescent layers but pyrolysis data were also obtained for BSF layers rich in organic matter 1-2 cm above and below luminescent layers (samples A and C, Table 4).

During routine core studies highly luminescent layers were observed under UV light. These luminescent layers and laminations usually have a thickness of 2-3 cm, sometimes reaching 5-6 cm, and appear to correspond to clay-rich argillites rather than the clayey-silty siliceous sediments that form the bulk of the BSF. Samples were taken of luminescent argillite material and associated clayey-silty siliceous shales from cores recovered from 10 separate wells in the central part of the BSF. Wells P-1, S-2, L-3, K-4 and V-5 are situated in the central part of the West Siberia Basin traversing from west to east. Wells R-6, E-7, G-8, M-10 and D-9 cover the south-east margin of the basin. In well D-9 we have found two layers with luminescence properties: an upper thin layer with a thickness of 5-10 mm and a lower layer composed of a series of numerous thin layers totally a thickness of about 5-6 cm (Fig. 3).

Geographically all these wells are situated within the limits of the Tomsk region and the Khanty-Mansi Autonomous Area (KMAO) area of the Russian Federation (Fig. 3).

3. Methods

3.1. Optical Microscopy

Geological samples were prepared into standard thin sections. Sections were polished down to 1um with diamond finished and carbon coated (Cressington 108 carbon sputtering unit) with a 20nm thickness. Thin sections of core samples from both the clayey-silty siliceous rocks and the luminescent layers were studied by optical microscopy using an Olympus BX-51 polarizing microscope. The samples were studied in plane polarized light under crossed polars so as to characterize the mineralogy (both authigenic and detrital minerals), as well as the organic and inorganic fine-grained phases, paying particular attention to textural and structural features.

3.2. Fluorescence Spectroscopy

Sections of core samples were viewed using a Leica DM5000B optical microscope (HC Plan 10x/0.30 PH1 objective) under epi-fluorescence using filter L5 (excitation 480/40 nm, emission 470 nm, dichroic mirror 505 nm) and images captured using a DFC310FX camera.

3.3. Scanning Electron Microscopy

Scanning electron microscopy was carried out at the electron microscopy facility (Durham University) using an Hitachi SU70 analytical high resolution electron microscope equipped with an Oxford Instruments Aztec 3.3 energy dispersive spectra (EDS) microanalysis system. Samples were investigated at 15kev and 0.74nA for both back-scattered (BSE) imaging and EDS identification.

3.4. Transmission Electron Microscopy

Fractionated clay samples (<2µm) of the luminescent layers were examined by TEM. Samples were prepared by dispersing in methanol and in distilled water and pipetting single drops of the suspension onto copper TEM grids with holey carbon supports. The samples were examined using bright field imaging at 200kV using an FEI Tecnai TF20 field emission TEM/STEM. Energy dispersive X-ray (EDX) spectra were obtained using an Oxford Instruments XMax80 Silicon Drift Detector and processed using Aztec software, whilst selected area electron diffraction patterns were recorded using a Gatan Orius SC600A CCD camera.

3.5. X-Ray Diffraction

The mineral composition of the luminescent layer samples was investigated by X-ray diffraction methods using a Rigaku Ultima IV powder diffractometer. Bulk samples were prepared by crushing selected core material followed by gentle grinding in a mortar with further grinding in McCrone mill to a particle size less than approximately 10µm. Randomly oriented powder samples for XRD analysis were prepared following spray-drying according to the recommendation of Hillier (2003). Clay fractions (<2µm) were collected from aqueous dispersions following treatment with hydrogen peroxide and sodium hypochlorite to remove organic matter. This treatment proved to be ineffective and more complete dispersion was only achieved following treatment with domestic detergent. Oriented samples were prepared by drying the dispersed clay on to glass slides. These samples were then examined by XRD in air-dried and ethylene glycol solvated states and after heating up to 550°C due to 2 hours. The XRD-patterns were measured using a Cu anode at 40 kV and 30 mA. Quantitative mineralogical analyses for the bulk samples were performed by Rietveld analysis (Bish and Post, 1993) using PDXL and Siroquant software (Taylor, 1991).

3.6. Fourier Transform Infra-Red (FTIR) Spectroscopy

1mg of each of the treated and separated clay fractions of the luminescent layers was incorporated in a potassium bromide pressed disc and Infrared (IR) spectra recorded over the frequency range 4000-400cm^{-1} using a Nicolet Magna-IR 550 (Thermo Scientific) Fourier Transform Infrared Spectrometer. The IR spectra were compared with reference spectra recorded from standard minerals.

3.7. Trace Element and Selected Major Element Analysis

The concentrations of 29 elements for 6 representative luminescent layer samples were determined using instrumental neutron-activation analysis (INAA) at the Nuclear Geochemical Laboratory of the Department of Geology of Tomsk Polytechnic University in Russia. The same 6 samples were additionally analyzed by ICP-MS for 53 trace elements. The samples were ground to ≤0.071mm and dissolved in a mixture of concentrated nitric, hydrofluoric, and hydrochloric acids. The ICP-MS analysis was done on the ELAN DRC-E equipment at the Chemical-Analytical Center “Plazma”, Tomsk. Determinations were made of the concentrations of Nb, Y, Zr, Ti, as well as some other elements, which are important for the identification of the initial magma composition from which volcanic ash is derived.

3.8. Pyrolysis Analysis

Pyrolytic analyses of samples of bulk luminescent rock samples were performed according to the procedures of RockEval 6 so as to enable further characterization of the organic matter fraction (Espitalie et al., 1985).

3.9. CHSN Analysis

The total percentages of carbon, hydrogen, nitrogen and sulphur were determined using a CHNS analyzer (Thermo Flash EA 2000, Thermo Fisher Scientific, Italy). For the CHNS analysis, freeze-dried and crushed samples were weighed (2–4 mg) and mixed with an oxidizer (vanadium pentoxide) in a tin capsule, which was then heated in a reactor at 950°C. The reaction of oxygen with the tin capsule at high temperature leads to raising the temperature in reactor up to about 1800 °C. At high temperature both organic and inorganic substances are converted into CO_2, H_2O, SO_2 and NO_2 (NO_2 is further reduced in the reactor), which are separated in a chromatographic column and detected by a thermal conductivity detector (TCD). The analyzer was calibrated using various samples of standard organic substances for quantitative determination of C, H, S and N. All samples were taken from luminescent argillite layers.

4. Results

Routine study of well core material recovered from the sediments of the Bazhenov suite is normally carried out by photographing the core under ultra-violet radiation (UV). This procedure aims to identify the presence of hydrocarbons (HC) that are known to luminesce under UV radiation. Carbonates also often luminesce under UV radiation in core material in different colors from bright yellow to bright red. On many occasions, however, the nature of the luminescence in the BSF is unknown and cannot be related to either carbonate layers or the presence of hydrocarbons. Thus, under UV radiation intensely luminescent layers were observed within the BSF both as single layers and as thin multiple laminations (up to a millimeter in thickness) within a small interval (Fig. 2).

4.1. Optical Microscopy

In general, the BSF is mostly made up of clayey-silty siliceous rocks, which may be regarded as silicites or radiolarites, containing rare layers of carbonate-rich material. Petrographically,

these rocks consist of fine micro-grain siliceous aggregates (35-40%), clay material (30-35%), with terrigenous detrital silty admixtures (up to 10-15%). The detrital admixture is distributed irregularly, forming fine silty lenses and powdery layers, consisting of quartz and feldspar detritus. Authigenic minerals include sulphide (pyrite and marcasite, sometimes up to 7-10%) and isolated grains of calcite, which are irregularly distributed within the rock. Organic matter (kerogen) is present in both concentrated form and dispersed as elongated and thread-like inclusions that form discrete red-brown and ginger-coloured layers. These formations are distributed regularly or in a layered way and colour the rock in shades of dark brown in polished sections, indicating their organic-rich nature.

In contrast, the luminescent layers tend to be much lighter in colour in polished sections suggesting an organic-poor nature (Fig. 1). Moreover, optical microscopy showed that the luminescent layers had a completely different fabric and micro-structure from that of the general sequence. Thin sections were made of the different components making up a complex of thick and thin luminescent layers. All layers showed a fabric consistent with that of poorly sorted, volcanic ash particles accompanied by a simultaneous accumulation of normal sedimentary material (Fig. 4). The meta-tuffites could possibly be related to the volcanic activity of Late Jurassic age that has recently been shown to have occurred in the Shadoron area of South East Transbaikalia (Stupak et al., 2016). For the most part, the luminescent layers are interpreted as consisting of meta-tuffites and could be regarded as a K-bentonite or a kaolin rich K-bentonite. The main mass of these rocks looks to be made up of devitrified glass in flattened and sinuous aggregates that could not possibly result from epiclastic sedimentary processes. The spatial distribution of the volcanic detritus corresponds to the structure of “plate stack” and shows that this rock debris has a flattened shape in cross-section but is isometric when observed perpendicular to the stratification. Quartz crystals are observed within the volcanic detritus, some with sharp angular edges and needle shapes and

occasional high temperature twins of Dauphiné type. Feldspar crystals are also observed with occasional polysynthetic twins. Dolomitized debris is common in the luminescent layers and organic matter is usually low, although some layers have a high OM content.

4.2. Fluorescence Microscopy

Observations with the fluorescence microscope showed that the luminescent layers are made up of discrete particles of diverse morphologies including rough lozenge-shapes, flattened discs and sinuous threads (Fig. 5a). These morphologies are clearly very similar to the meta-tuffite particles observed by optical microscopy as illustrated in Figure 4. The contrast between the luminescent argillite and the adjacent clayey-silty siliceous rock is vividly illustrated by Fig. 5b.

4.3. Scanning Electron Microscopy

Back-scattered SEM images from polished thin sections of a clay-rich luminescent sample of the BSF are shown in Fig. 6. Two morphologically distinct phases are immediately evident. The first consists of blocky crystalline aggregates, some 5 to 10 µm in length, which can be seen to be delaminating along basal surfaces into units <2µm in thickness. These aggregates yield EDS consisting only of Si and Al peaks in about equal intensity and enable their identification as a kaolinite. The second phase consists of a continuous mass of clay minerals, with boundaries that are a change in texture from the kaolin mineral. EDS shows that this material is also aluminous but with significant peaks of K and Mg and is identified as a illite and illite-smectite clay minerals (Fig. 6c). Pyrite is certainly authigenic, forming in framboidal aggregates in the relatively anoxic environment of the deep marine sediment

4.4. Transmission Electron Microscopy

The ostensibly pseudo-fibrous nature of the mixed-layer I/S clay material in the luminescent argillite which is suggested by the SEM micrographs is not confirmed by TEM examination. In fact, most of the dispersed particles have an irregular, indeterminate, platy morphology and no clearly fibrous particles are to be seen (Fig. 7). However, most of these particles are clearly aggregates made up of smaller particles, usually of equally indeterminate morphology, although occasional laths and hexagonal kaolinite-like fragments can also be seen. Platy particles with curled edges and some fully rolled up laths, which could in principle be mistaken for fibrous particles, are also evident. Some aggregates appeared to show a substructure of lath-like particles and at the edge of these aggregates a hexagonal single crystal electron diffraction patterns were recorded (Fig. 8a and 8b). However, a turbostratic-type selected area electron diffraction pattern, typical of smectite aggregates where the structural sheets are arranged at random with respect to the electron beam, was recorded from aggregates of platy particles (Fig. 9a). Spacings of 4.20 to 4.40Å characteristic of a dioctahedral mica mineral were measured from this pattern. This suggests a similar random orientation of whatever structural units are making up the platy particle. In Fig. 9b, the (00l) and (hk0) d-spacings were measured at 10.3 and 4.40Å respectively, also characteristic of mica type mineral. A qualitative EDS analysis of these regions gave the following results (in atomic %): Si 18.8%; Al 12.1%; K 1.2%; Mg 1.1%; Ca 0.2%; Fe 0.1% and O 66.6%.

4.5. X-Ray Diffraction

XRD showed that the luminescent argillites are significantly more clay-rich than in the normal BSF sequence and that two main types can be distinguished, namely (1) luminescent layers rich in kaolinite minerals and (2) luminescent layers also yielding a strong reflection at 11.3Å which expands to 12.1Å after ethylene glycol treatment signifying a mixed-layer

illite/smectite. Quartz, feldspars, carbonates and sulfides are present as minor phases (Table 1). The luminescent argillite layers all have a clay content determined by XRD (Kaolinite + I/S) of between 70 and 80% whereas the host clayey-silty rocks of the Bazhenov Shale have an average clay content of only 22.91% (Zanin et al., 2008). The country rocks of the non-luminescent materials, the main phase of the BSF, are siliceous materials sometimes with anomalous contents of carbonates, mainly dolomite (Compare Tables 1 and 2).

Figure 10 shows an XRD pattern of a luminescent layer that is kaolinite-rich. The kaolinite is evidently a well crystalline variety as shown by the sharpness of the diffraction peaks as well as the good resolution of the hkl peaks in the 4.36-4.12Å range. The XRD pattern for dickite shows that the two strongest diagnostic reflections for dickite occur at 3.79 and 3.43Å (Wilson, 2013) but only one of this reflections (3.79Å) has been found. Other hkl reflections correspond with well-crystallized kaolinite and it is concluded that the sample consists mainly of kaolinite, although we do not exclude a combined composition for the kaolin-rich layer consisting of mainly kaolinite with at least some dickite stacking.

Figure 11 shows oriented XRD patterns of a luminescent layer with a felted, pseudo-fibrous appearance following air drying, glycolation and heating to 550°C. It is evident that kaolinite is minimal in this sample and that the effect of glycolation is to expand the major peak at about 11.3Å to about 12.1Å, a response normally construed as indicating the presence of smectite interlayers. This interpretation was confirmed by the result of heating to 550°C which brought about a contraction of the main reflection at 11.3Å to about 10.1 Å. It would seem, therefore, that the results can be interpreted as a mixed-layer illite-smectite (I/S) but there were no matching calculated curves illustrated in either random or ordered forms in Reynolds (1980) or in Moore and Reynolds (1997). However, Hong et al. (2016) recorded similar spacings from air-dried and ethylene glycol solvated clay fractions from altered

Permo-Triassic volcanic ashes in Guizhou Province, South China, and using the NEWMOD program for Windows (Reynolds and Reynolds, 1996) obtained matching experimental and calculated one-dimensional XRD patterns for ordered R3 and R2 I/S structures (~90/10 up to 75/25). An alternative explanation could be that the I/S mineral consists largely of a simple R1 stacking sequence, which is interrupted by discrete sequences of illite layers, rather than a complex of R2 and R3 stacking sequence as described by Hong et al. (2016).

4.6. Infrared Spectroscopy

Figure 12a shows an IR spectrum obtained after separation of the clay fraction of a luminescent layer from non-clay minerals and organic compounds. The pattern is characterized by intense OH-stretching bands in the 3600-3700 cm^{-1} range. The relative intensities of these bands match the spectrum for dickite shown by Russell and Fraser (1994) more closely than they do that of kaolinite (Fig. 12b and 12c). In particular, in dickite Russell and Fraser (1994) recorded a band at 3704 cm^{-1} which they attributed to internal surface OH groups, whereas in the luminescent layer clay this band occurs at 3689 cm^{-1}, which is closer, although not identical to that yielded by kaolinite. The OH deformation bands occurring at 936 and 910 cm^{-1} in the luminescent sample are not diagnostic and could be attributed to either kaolinite or dickite.

Also present in the spectrum is a weak absorption band at 1423cm^{-1}. This could be due to carbonate, as calcite is present as a trace constituent in some of the luminescent layers, or to the NH_4^+ cation which could be located in the interlayer space of the mixed-layer I/S phase. Heating experiments favour the latter interpretation, as calcite decomposes to release CO_2 on heating to ~ 850 to 900°C while the interlayer NH_4 decomposes to NH_3 following heating at 530-570°C (Higashi, 1982). As can be seen from Fig. 18 the absorption band at 1432cm^{-1} disappears from the spectrum between 500 and 700°C.

4.7. Trace Element and Selected Major Element Analysis

The trace element chemical composition of the luminescent argillites is as well as the clayey-silty siliceous rocks of the Bazhenov Shale similar to the average composition of sedimentary rocks (Grigor'ev, 2003, Rikhvanov et al., 2015), but the samples are also characterized by some specific peculiarities. Their most noticeable feature is a high content of the radioactive elements uranium and thorium (Table 3), which is similar to the content of the Bazhenov suite. These uranium anomalies were studied by Baturin (1975) and Kochenov and Rasulova (1978) who showed, using examples from modern marine basins, the key role of organic matter in uranium accumulation. A high content of As and Se is also indicative of the supergenetic nature of uranium accumulation, which often accompanies hydrogenous deposits of uranium in a reducing environment. According to Spears (2017), the same assemblage (As, Se, Sb, Cu, Pb, Tl, Cd and U) is typical for marine shales and marine-influenced coals. High thorium content in the hypergenetic zone of marine sediments is primarily indicative of mechanical accumulations in the coastal zone of monazite placers and other stable thorium-bearing heavy accessory minerals. Leaching of mobile elements from marine suspension and the relatively slight increases in the concentrations of the other slowly moving hydrolysable elements during hypergenesis could explain their insignificant accumulation and a composition that does not differ much from bulk sedimentary rock values. Moreover, the luminescent layers do not show contrasting anomalies of these elements, indicating sedimentation of material that was primarily enriched with thorium. This material could have been derived from some initially thorium-enriched crusts of weathering or from thorium-enriched volcanogenic pyroclastic materials. Here, a volcanogenic source appears more likely source, as thorium-bearing horizons are found extending along hundreds of kilometers at a small but constant thickness. This mode of substance distribution is consistent with catastrophic phenomena such as simultaneous ash falls over a large territory.

The content of individual REE in luminescent layers and the course of their normalized distribution curves confirm a clastogenic mechanism of their accumulation. The concentration of light REEs is close to their content in volcanic rocks of acidic and intermediate igneous nature, but for the heavy REEs is significantly lower. One possible reason is loss of heavy REEs during sediment leaching. It is known that heavy REEs readily form complexes with organic ligands and could thus be extracted from the luminescent layers. The low Eu content indicates either an intermediate or weakly-acidic composition of the initial pyroclastics, corresponding to andesites, dacites, rhyodacites, etc. and this is also consistent with the low content of Fe, Co, Ni.

4.8. Pyrolysis Studies

Pyrolytic analyses of luminescent argillites (B) and clayey-silty siliceous rocks above (A) and below (C) these argillites are shown in Table 4. Pyrolysis was also performed on the same samples after exhaustive extraction with chloroform in a Soxhlet apparatus (40hrs extraction). It is important to note that all luminescent samples retained their luminescence after extraction, confirming that the luminescence phenomenon is not related to the presence of the free hydrocarbons extracted by chloroform.

The clayey-silty siliceous rocks under study have a high oil-generating potential (S2>20 mg/g; TOC>4%). Their organic matter (OM) possesses a very high oil-generating quality as characterized by its high hydrogen index (for example, HI>700mg of HC/g TOC at low maturity Tmax<435°C). The high quality organic matter and strongly reducing conditions of sediment formation are consistent with low values of oxygen index (OI, Table 4). An increase in the maturity parameter Tmax brings about decreasing HI (Fig. 13b). The productivity index (PI = S1/(S1 + S2)) of these rocks rarely exceeds 0.10 (Table 4), which corresponds to the beginning of the “oil window”. After extraction the S2 and HI parameters

slightly decrease for the samples (Fig. 13). Here, the higher the maturity of OM, the larger the change in the parameters, thus indicating a higher content of free generated HC (bitumoids).

The argillite luminescent layers show a much lower content of total organic carbon (TOC) compared to the adjacent bituminous clay-silty siliceous layers (Table 4, Fig. 13). The oil-generating potential of the luminescent layers is rather poor (S2>2.5 mg/g; TOC>0.5%). Their hydrogen index (HI) changes over a wide range of values from 150 to 500 mg HC/g TOC and does not depend on the Tmax parameter. Also, Tmax values are really low for some individual samples (<410°C), which is perhaps caused mainly by the presence of free HC (bitumoids) in the layers with low oil-generating potential. This is also consistent with the very high values of the productivity index PI and the correlation between PI and Tmax (Table 4). It is possible that these free HC are not genetically bound to the OM of these samples and are naturally migratory.

In contrast to the luminescent layer samples before extraction, the Tmax values of these samples after extraction are not extremely low and their Tmax values become closer to each other (Fig. 13b). However, there is still no correlation between HI and Tmax for the luminescent argillites after extraction, as opposed to the adjacent clayey-silty siliceous rocks of the Bazhenov suite. The results suggest that the organic matter in the luminescent argillites was not only depleted (diluted) by an abundant quantity of mineral (ash) material delivered to the basin, but that its quality (HI) was also affected by different mechanisms of OM transformation during sedimentation and diagenesis. Variations of oxygen index (OI) are consistent with the effect of these changing factors as well as the levels of depletion (dilution) from one episode to another during accumulation of the luminescent layers.

4.9. Gas Analysis

Analysis for the primarily organic elements are listed in Table 5 in relation to the clay mineralogy of luminescent layers. The results appear to be highly variable and are discussed below.

5. Discussion

5.1. Nature of luminescent layers in the BSF

Optical microscopy leaves little doubt that the luminescent layers in the argillites of the BSF are in large part made up of volcanic material, as indicated by the intensely deformed and elongated shapes of their constituent particles and the specific micro-textures formed by these constituents. It is considered that many of the particles seen under the optical microscope represent devitrified volcanic glass and that the rock making up the luminescent layers can be described as a meta-tuffite. Van (1973) has shown that ash falls were widespread events throughout the Jurassic of the West Siberia basin. However, at the same time that these ash falls were taking place, the depositional sites of the luminescent layers were also receiving detrital inputs of silty material such as are characteristic of the BSF as a whole. It is envisaged that the ash falls acted as a single top-cutting influx of extraneous sediments into the predominantly silty material of the BSF.

Quantitative XRD shows that the luminescent layers are clay-rich (Table 1) and contain two types of clay minerals, namely a kaolin-rich mineral and a mineral which was identified as an ordered mixed-layer illite/smectite (Fig. 10 and 11). The kaolin mineral has a diffraction pattern consistent with well-ordered structure, but possibly with some dickite stacking. IR spectroscopy yields spectra in the OH-stretching range which are shown presence a dickite not only kaolinite (Fig. 12) and SEM images show that the kaolin mineral has a blocky structure built up of large aggregated stacks of crystals (Fig. 6a), which is also typical of for

dickite. It was concluded that the kaolin minerals in the luminescent layers consists of normal well-crystallized kaolinite with some dickitic layers.

XRD shows that some luminescent argillites contain a phase yielding a peak at 11.3Å which glycolation causes to expand to 12.1Å and heating at 550ºC brings about contraction to about 10.1Å (Fig. 11). SEM images of thin sections of a luminescent sample rich in this material show a surface texture consisting of felted mass of tangled, interwoven pseudo-fibres as described above. EDS analysis shows this material to be highly aluminous with significant K and Mg, although some other areas are richer in Mg and Fe and contain correspondingly less Al. The presence of K in the EDS spectra of this material suggests that it is the dominant interlayer cation in the ordered mixed-layer I/S identified by XRD. That the K ion is indeed associated with pseudo-fibrous material can be seen in the element maps of Fig. 14 showing the distribution of elements that make up the major clay minerals in the luminescent layers.

TEM studies tend to confirm these observations but add other important details. In particular, it can be observed that the dispersed clay fraction of a luminescent layer rich in mixed-layer I/S consists of platy particles of irregular outline but with a substructure of lath-like particles in various orientations. Therefore, the dispersion appears to have been incomplete and the particles are still in an aggregated form (Fig. 7 and 8a). Thin laths at the edge of the aggregated particles yield a hexagonal single spot ED pattern and are therefore truly crystalline with 3-dimensional periodicity (Fig. 8a and 8b). Curled lath edges and aggregated particles yield ED patterns which may be described as turbostratic (continuous rings) as shown in Fig. 9a, although a degree of coherent stacking may be shown by rows of discrete but streaked hkl reflections as in Fig. 9b. These rolled up laths yield (00l) reflections of 10.2-10.3Å and contain K (as well as Si and Al) and are therefore typically micaceous in structure.

Non-clay minerals identified by EDS in the luminescent layers include pyrite, which yields a spectrum consisting only of Fe and S peaks, and reaches a total of up to 5%. Calcite was also identified by intense Ca and C peaks but must be a relatively minor phase as it was listed as present by XRD in only two samples under study. In conjunction with morphology as shown by SEM, quartz and feldspars were also distinguished by EDS analysis (Table 1).

Table 4 shows that the TOC in the luminescent argillites is much lower than that of the clayey-silty siliceous sediments above and below them. The nitrogenous nature of the organic matter in the luminescent argillites is noteworthy and calls for some explanation. In its initial OM bioproduct state, nitrogen is present in proteins and amino acids which normally decay during sedimentation. Depending upon the duration of the OM in its suspended state in the oxygen saturated water, the proteins are either fully or partly lost. A characteristic feature of sediment formation in the BSF is the strong reducing conditions where much of the nitrogen is preserved in proteins. This leads to high nitrogen content in kerogen (Bogorodskaya et al., 2005), as well as in the oils based on them (Goncharov, 1987). During diagenesis some nitrogen is likely present in the nitrogen-containing organic structures of kerogen, which can be closely associated with the clay surface by adsorption. It is worth mentioning that luminescence phenomena observed in the clay phase of coals (Hessler, 1989) and kaolinite pastes (Coyne et al., 1981; 1984) indicate a close bonding of nitrogen aromatics to mineral surfaces. Langford and Blanc-Valleron (1990) analysed the amount of pyrolysable organic material by plotting S2 vs TOC for numerous shale samples. They found that in most cases the organic matter is not completely pyrolysed and that the regression line does not pass through the origin but intercepts the x axis. This is consistent with some resistant organic matter being adsorbed by clay. Similarly, when S2 was plotted against TOC for the luminescent layers it was again found that the regression line did no quite pass through the origin but intercepted the x axis indicating that about 0.5% organic matter was present,

presumably adsorbed on clay (Fig. 15). Although this may not be statistically significant it should be recalled that gas analysis of the luminescent layers (Table 5) indicated the presence of nitrogenous organic matter.

Nitrogen compounds from kerogen have mostly pyrrolic and pyridinic structures (Bennett and Love, 2000) and fall in the range of organics studied by Coyne and co-authors (1981; 1984), which are found to promote the luminescence of kaolinite clay. The distribution of organic compounds in source rocks and related crude oils have shown large and systematic variation due to fractionation effects associated with the primary and secondary migration processes (Yamamoto, 1992; Li et al., 1995). Bennett and Love (2000) studied samples of the Kimmeridge Clay Formation and identified a significant range of nitrogen-containing organic compounds and concluded that this indicates the formation of nitrogen compounds at a relatively early stage of diagenesis. This possibly suggests that similar nitrogen compounds may occur in the luminescent layers of the BSF which is close to the stratigraphic equivalent of the Kimmeridge Clay.

5.2. Origin of the luminescent layers

The evidence outlined above indicates that some specific luminescent layers in inter-bedded argillites of the BSF can be described as meta-tuffites and are analogous to K-bentonite (kaolinitic K-bentonite) and are composed primarily of volcanic ash material, but with a significant contribution of silt-sized minerals of terrigenous origin that are typical of the BSF as a whole. The clay mineralogy of these luminescent layers is undoubtedly almost exclusively authigenic in origin as shown by the extraordinary morphology of the kaolinite/dickite and ordered mixed-layer I/S clays which is clearly incompatible with normal detrital sedimentation. As for the conditions under which the kaolin minerals formed, although Ehrenberg et al. (1993) suggested that kaolinite transformed to dickite at about 3 km

depth at temperatures of 120-130ºC in Mesozoic sandstones of the North Sea, later studies by Beaufort et al. (1998) and Lanson et al. (2002) suggest that a progressive transformation to dickite can occur at lower temperatures and more shallow depths as a result of kinetic and other factors.

With regard to the origin of the ordered mixed-layer I/S mineral, the conventional wisdom at the present time is that this develops from a smectitic precursor from randomly ordered mixed-layer illite-smectite at temperatures in the 80-90ºC range, either by a layer-by-layer transformation of smectite to illite or by a dissolution/precipitation mechanism (Środoń et al., 2009; Wilson, 2013 and references therein). The fact that the luminescent layers are to a large extent derived from altered volcanic ash, and are therefore likely to have provided smectitic clays through the alteration of volcanic glass, may be viewed as supporting this general concept.

The possibility that the kaolinite and ordered I/S minerals may be a direct cause of luminescence should be considered, particularly bearing in mind the findings of Götze et al. (2002) that in general all dioctahedral clay minerals show visible cathodoluminescence (CL) whereas the trioctahedral clay minerals do not. Both kaolinite and dickite minerals show a characteristic deep blue CL and, as noted above, the ordered I/S clay mineral also has a dioctahedral structure. Walker and Burley (1991) recorded bright, sky blue CL emission as typical of pore-filling and grain replacing kaolinite and noted that kaolinite showed a broad emission band at ~400nm and a distinct shoulder at ~350nm in the UV at room temperature. They further noted that at least half of the CL intensity of this broad band was emitted in the UV. Götze et al. (2002) observed that the characteristic blue CL of kaolinite and other dioctahedral minerals was caused by an intense emission band at ~400nm, comprising a double peak at 375 and 410 nm respectively, and related this to radiation-induced defect

centres, probably related to silicon-oxygen (Si – O) or aluminium-oxygen (Al – O – Al) bonds (Götze, 2012). Such defects are usually induced by bombardment of alpha particles (Marshall, 1988). Table 2 shows that the luminescent layers contain radioactive elements, as determined by two methods of analysis, at concentrations far above those normally encountered in shales. Thus, the luminescent layers dominated by well crystalline kaolin minerals contain uranium ranging from 11 to 67 ppm and thorium from ~1 to 76 ppm. Where the luminescent layers contain both kaolinite and ordered mixed-layer I/S clays uranium ranges from 20 to 80 ppm and thorium from 32 to 77 ppm.

Bearing in mind that the luminescent argillites are more clay-rich than the clayey-silty siliceous sediments of the BSF as a whole, and that the clay minerals that they contain have an extraordinary authigenic morphology and were derived from altered volcanic ash, then it would seem logical to relate these special factors to their luminescent characteristics in the UV. It should be noted, however, that while well crystalline kaolin minerals occurred in the luminescent layers in all of the 10 cores studied, the ordered mixed-layer I/S mineral occurred only in 6 of them. Therefore, the presence of well crystalline kaolinite (with at least some dickite additives) is a common factor in the luminescent layers and on this basis is thought to be the major contributor to the luminescence of the argillites in the BSF.

However, a possible role for organic matter, whether in discrete form or adsorbed on clay, in giving rise to the luminescence is also worth examining in more detail, even though the argillites have a much lower TOC than the non-luminescing sediments immediately above and below them (Table 4). Nevertheless, the small amount of organic matter present in the luminescent layers is unexpectedly quite nitrogenous in some samples (Table 5), suggesting a possible genetic link with luminescence. It is envisaged that in the initial bio-product state of organic matter, nitrogen was present as proteins and amino acids which would normally

quickly decay when present in the oxygenated upper water column. However, because the luminescent layers are derived from volcanic ash, it is possible that the ashy sediment could transit more quickly through the oxygenated layers of the water column entraining within it some of the suspended relatively fresh organic matter. Once deposited on the deep-sea floor, this organic matter was preserved by the strongly reducing, anoxic conditions that are characteristic of the BSF, and possibly by adsorption on to clay minerals.

To clarify the question of whether the luminescence in the argillites was due to organic matter or to the nature of their clay minerals, a luminescent sample was heated at 400, 500, 700, 800 and 900°C. After heating to each temperature, the luminescence of the sample was photographed under day light and UV (Fig. 16) and then analysed on an FTIR-spectrometer (Fig. 17). The sample photographed under UV showed that the intensity of luminescence significantly decreased around 400°C and practically disappeared at 500°C. Although this result might be reasonably attributed to the thermal decomposition of organic matter, beginning at ~300°C and completed at 500°C, it is also consistent with the observation that the luminescence in most materials decreases with increasing temperature (Marshall, 1988). Also, it is noteworthy that although the clayey-silty siliceous rocks of the BSF contain abundant nitrogenous organic matter, they do not luminesce under UV in the same way as the luminescent layers in the argillites. It is concluded, therefore, that the luminescence of the argillite layers is more likely to be related to clay mineralogy rather than to organic matter. However, the latter cannot be completely discounted as accounting for at least some of the luminescence.

5.3. Significance of the luminescent layers

If the luminescent layers are accepted as having formed from volcanic ash falls of wide lateral extent, and that it is reasonable to describe them as meta-tuffites, then there is a wide

possible range of alternative names. For example, the illite-smectite type illustrated by upper layers in Figure 3 could be regarded a K-bentonites, while the kaolin type in the lower layers shown in Figure 3 could be regarded as kaolinitic bentonites. Because they have a unique position within the Bazhenov Shale Formation in general then it is evident that they could be as useful in oilfield exploration as tonsteins and K-bentonites are in coalfield and other geological explorations (Środoń, 1972; Somelar et al., 2009; Warren, 2016; Dai et al., 2017). In fact, the characteristics of the luminescent layers can be usefully compared with those of tonsteins in that they both derive from laterally extensive ash falls that have been altered to highly crystalline kaolin minerals in a strongly reducing environment. A plot of the Zr/TiO_2 and Nb/Y ratios of luminescent layer samples on the magmatic discriminant diagram of Winchester and Floyd (1977) places them in the Rhyo-dacite/Dacite field (Fig. 18). Such a magmatic source is relatively high in Al and it seems probable that this could explain the high alumina clay minerals in the luminescent layers. However, the differences between the luminescent layers and tonsteins are equally significant. Tonsteins have formed at or very near land surface whereas the luminescent layers of the argillites, in common with much of the BSF, are deep water deposits.

Spears (2012) pointed out that the evident stratigraphic value of tonsteins has been much enhanced by recent geochemical studies, particularly those involving radiometric age dating and detailed trace element analysis. These studies suggest that a chemostratigraphic approach can be used to characterize and identify particular tonsteins, thus providing useful benchmarks in coalfield exploration. Evidently, the luminescent layers in the BSF may also have the potential to be used for exploration of hydrocarbons in a similar way. We are only at the beginning of such activity compared with tonstein studies which have been proceeding for well over a century.

It should be emphasized that the clay mineralogy of the luminescent layers may well be sensitive to environmental changes, involving possible dickitization of kaolinite with concomitant formation of ordered mixed-layer I/S, with both processes being able to relate to the position of the adjacent sediments to the oil window. It is concluded, therefore, that wider and more systematic study of the mineralogy and geochemistry of the luminescent layers of argillites in the West Siberian Basin may be a worthwhile exercise in the search for new hydrocarbon resources.

6. Conclusions

Luminescent layers of unusual intensity under UV radiation occur in argillites in the Bazhenov Shale Formation (BSF) of the West Siberia Basin and extend over a wide lateral area of more than hundreds of square kilometers. Optical microscopy shows convincingly that these layers represent altered volcanic ash falls and may be described as meta-tuffites or K-bentonites. The luminescent layers are clay rich but deficient in organic matter compared with the sediments above and below them. The main clay minerals in the luminescent layers are a kaolin mineral consisting of kaolinite with a certain amount of dickite additives, as well as an ordered mixed-layer illite-smectite (I/S) which occurs in aggregates of distinctive felted masses. Both clays are of authigenic origin and were derived from altered volcanic ash material. The origin of the unusually intense luminescence under UV of the argillites in the Bazhenov Shale is broadly related to their dioctahedral clay mineralogy, but especially to its content of well crystalline kaolin minerals due to radiation induced defects brought about by theit high uranium and thorium contents. In some ways the luminescent layers may be compared with tonsteins and K-bentonite spread located in different geological environment especially with regard to their general stratigraphic significance, and the fact that they contain

a clay mineral suite that is temperature sensitive suggests that their systematic study may prove useful in the search for hydrocarbon deposits in the BSF.

Acknowledgments

Investigations of clay minerals were partially carried out within the framework of IGEM RAS № 0136-2018-0024

The authors would like to express their gratitude to G.J. Russell for his help with SEM data, Fedunina N.V. (Chemical-Analytical Center "Plazma"), for her help with the ICP-MS analysis and A.F. Sudyko for his assistance with INNA for trace, and rare earth element analyses. We are also grateful to Prof. Ward and an anonymous reviewer for their constructive comments and suggestions.

References

Baturin G.N., 1975. Uranium in recent marine sedimentation. Moscow, Published by Atomizdat, 152 pp. (in Russian).

Beaufort, D., Cassagnabere, A., Petit, S., Lanson, B., Berger, G., Lacharpagne, J.C., Johansen, H., 1998. Kaolinite-to-dickite reaction in sandstone reservoirs. Clay Minerals. 33. 297-316. http://dx.doi.org/10.1180/claymin.1998.033.2.12

Bennett, B., Love, G.D., 2000. Release of organic nitrogen compounds from kerogen via catalytic hydropyrolysis. Geochem. Trans., 10, 61-67. http://dx.doi.org/10.1039/b008675o

Bish, D.L., Post, J.E., 1993. Quantitative mineralogical analysis using the Rietveld full pattern fitting method. American Mineralogist, 78, 932–940.

Bogorodskaya, L.I., Kontorovich, A.E., Larichev, A.I., 2005. Kerogen. Methods of Study and Geochemical Interpretation, Novosibirsk: Geo, 254 pp. (in Russian).

Coyne, L.M., Lahav, N., Lawless, J.G., 1981. Dehydration-induced luminescence in clay minerals – relevance to prebiotic dehydration polymerization. Nature, 292, 819-820.

Coyne, L., Pollack, G., Kloepping, R., 1984. Room-temperature luminescence from kaolin induced by organic amines. Clays & Clay Minerals, 32, 58-66.

Dai S., Ward, C.R. Graham I.T., French D., Hower J.C., Zhao L., Wang X., 2017. Altered volcanic ashes in coal and coal-bearing sequences: A review of their nature and significance Earth-Science Reviews, 175, 44-74.

Eder, V.G., Zanin, Y.N., Zamirailova, A.G., 2003. Trace fossils of the Upper Jurassic Bazhenov and Georgiev formations of the West Siberian Plate. Russian Geology and Geophysics. 44, 517-524.

Ehrenberg, S.N., Aagard, P., Wilson, M.J., Fraser, A.R., Duthie, D.M.L, 1993. Depth dependent transformation of kaolinite to dickite in sandstones of the Norwegian continental shelf. Clay Minerals, 28, 325-352.

Einsele, G., 2000. Sedimentary Basins: Evolution, Facies and Sediment Budget. Springer, Berlin. 792pp.

Espitalié J., Deroo G., Marquis F., 1985. La pyrolyse Rock-Eval et ses applications. Premiére partie // Revue de l'Institut Francais du Pétrole, 40, 563-579.

Goncharov, I.V., 1987. Geochemistry of oil in Western Siberia, Moscow: Nedra Publishing House, 1987, 181 pp. (in Russian).

Goncharov, I.V., Samoilenko, V.V., Oblasov, N.V., 2014. Prospects for shale oil in Bazhenov Formation in the south-east of Western Siberia. SPE-171170 presented at the SPE Russian Oil and Gas Exploration and Production Technical Conference and Exhibition, Moscow, 14–16 October 2014.

Götze, J. 2012. Application of cathodoluminescence microscopy and spectroscopy in geosciences. Microscopy and Microanalysis. 18, 1270-1284.

Götze, J., Plötze, M., Götte, Th., Neuser, R.D., Richter, D.K. 2002. Cathodoluminescence (CL) and electron paramagnetic resonance (EPR) studies of clay minerals. Mineralogy and Petrology. 76, 195-212.

Grigor'ev, N.A., 2003. Average concentrations of chemical elements in rocks of the upper continental crust. Geochemistry International. 41, 711–718.

Hessler, R.K., 1989. Luminescence in coal and its relation to clay minerals. Clay Minerals. 34, 107-113.

Hillier, S. 2003. Quantitative analysis of clay and other minerals in sandstones by X-ray powder diffraction (XRPD). International Association of Sedimentologists. Special Publication. 34, 213–251.

Higashi, S., 1982. Tobelite, a new dioctahedral ammonium mica. Mineralogical Journal. 11, 138-140.

Hong, H., Fang, Q., Zhao, L., Schoepfer, S., Wang, C.C., Gong, N., Li, Z., Zhong-Qiang, Ch., 2017. Weathering and alteration of volcanic ashes in various depositional settings during the Permo-Triassic transition in South China: Mineralogical, elemental and isotopic approaches. Palaeogeography, Palaeoclimatology, Palaeoecology. 486, 46-57. http://dx.doi.org/10.1016/j.palaeo.2016.12.033

Jenkyns, H.C., Clayton, J.C., 1986. Black shales and carbon isotopes in pelagic sediments from the Tethian Lower Jurassic. Sedimentology. 33, 87-106.

Kochenov, A.V., Rasulova, S.D., 1978. On the conditions of uranium mobilization and accumulation during modern sedimentation. M. 12-21 (in Russian).

Kontorovich, A.E., Melenevskii, V.N., Zanin, Y.N., Zamirailova, A.G., Kazanenkov, V.A., Kazarbin, V.V., Makhneva, E.N., Yamkovaya, L.S., 1998. Lithology and formation conditions of basic rocks in the Bazhenov formation (West Siberia). Russian Geology and Geophysics, 39, 1477–1492.

Langford, F.F., Blanc-Valleron M.M., 1990. Interpreting RockEval pyrolysis data using graphs of pyrolysable hydrocarbons vs total organic carbon. American Association of Petroleum Geologists Bulletin, 74, 799-804.

Lanson, B., Beaufort, D., Berger, G., Bauer, A., Cassagnabere, A., Meunier, A., 2002. Authigenic kaolin and illite minerals during burial diagenesis of sandstones: a review. Clay Minerals. 37, 1-22.

Li, M., Larter, S. R., Stoddart, D., Bjorøy, M., 1995. Fractionation of pyrrolic nitrogen compounds in petroleum during migration: derivation of migration-related geochemical parameters Geological Society, London, Special Publications, 86, 103-123.

Marshall, D.J., 1988. Cathodoluminescence of Geological Materials. Unwin & Hyman, Inc, London. 146 pp.

Moore, D.M., Reynolds, R.C.Jr., 1997. X-ray diffraction and the identification and analysis of clay minerals, Oxford University Press, Oxford, NY, pp. 378.

Reynolds, R.C., 1980. Interstratified clay minerals. Chapter In: Crystal structures of clay minerals and their X-ray identification, Eds. G. W. Brindley and G. Brown. pp. 249-303.

Reynolds, Jr.R.C., Reynolds R.C.III, 1996. NEWMOD-for-Windows: The calculation of one-dimensional diffraction patterns of mixed-layer clay minerals. Hanover, New Hampshire.

Rikhvanov, L.P., Usoltsev, D.G., Ilenok, S.S., Ezhova, A.V., 2015. Mineralogical and geochemical features of the Bazhenov formation, West Siberia, according to nuclear physics and electron microscopic methods of research. Izvestiya TPU, 326 (1), 50–63.

Russell, J.D., Fraser, A.R., 1994. Infrared methods. In: Clay Mineralogy: Spectroscopic and Chemical Determinative Methods. (M. J. Wilson editor). Chapman & Hall, London. pp. 11-67.

Shaldybin, M.V., Lopushnyak, Y.M., Goncharov, I.V., Wilson, M.J., Wilson, L., Mendis, B.G., 2017.The mineralogy of the clayey-silty siliceous rocks in the Bazhenov Shale Formation (Upper Jurassic) in the West Siberian Basin, Russia: The role of diagenesis and possible implications for their exploitation as an unconventional hydrocarbon reservoir. Applied Clay Science. 136, 75-89. http://dx.doi.org/10.1016/j.clay.2016.11.009

Somelar P., Kirsimäe K., Środoń J., 2009. Mixed-layer illite-smectite in the Kinnekulle bentonite, northern Baltic Basin. Clay Minerals 44, 455-468.

Spears, D.A., 2012. The origin of tonsteins, an overview and links with seatearths, fireclays and fragmental clay rocks. International Journal of Coal Geology. 94, 22-31. http://dx.doi.org/10.1016/j.coal.2011.09.008

Spears, D.A., 2017. The role of seawater on the trace element geochemistry of some UK coals and a tribute to Goldschmidt. Minerals. 7, 148-163. doi:10.3390/min7080148

Środoń J., 1972. Comparative study of K-bentonite and coal-tonstein from the Upper Silesian Coal Basin, Poland. Bull. Acad. Polon. Sci., Ser. Sci. de la Terre 20, 165-173.

Środoń J., Zeelmaekers E., Derkowski A., 2009. Charge of component layers of illite-smectite in bentonites and the nature of end-member illite. Clays & Clay Minerals 57, 650-672.

Stupak, F.M., Kudriashova, E.A., Lebedev, V.A., 2016. On the Jurassic volcanism and on volcanoes in the Shadoron Basin, eastern Transbaikal. Journal of Volcanology and Seismology. 10, 86-99.

Taylor, J.C., 1991. Computer programs for standardless quantitative analysis of minerals using the full powder diffraction profile. Powder Diffraction. 6, 2–9.

Ulmishek, G.F., 2003. Petroleum geology and resources of the West Siberian Basin, Russia. U.S. Geological Survey Bulletin, 2201-G (49 pp).

Vyssotski, A.V., Vyssotski, V.N., Nezhdanov, A.A., 2006. Evolution of the West Siberian Basin. Marine and Petroleum Geology. 23, 91–126.

Walker, G., Burley, S.D., 1991. Luminescence petrography and spectroscopic studies of diagenetic minerals. In Luminescence Microscopy and Spectroscopy: Qualitative and Quantitative Applications. (C. E. Barker and O. C. Kopp., Editors). Short Course No. 25; Society of Economic Paleontologists and Mineralogists, Dallas, Texas, USA. pp 83-96.

Warren D. Huff, 2016. K-bentonites: A review. American Mineralogist. 101(1), 43-70. https://doi.org/10.2138/am-2016-5339.

Wilson, M.J., 2013. In Deer, Howie and Zussman, Rock-Forming Minerals, Sheet Silicates, Clay Minerals. Volume 3C. Geological Society, London, 732 pp.

Winchester, J.A., Floyd, P.A., 1977. Geochemical discrimination of different magma series and their differentiation products using immobile elements. Chemical Geology. 20, 325-343.

Yamamoto, M., 1992. Fractionation of azaarenes during oil migration. Organic Geochemistry, 19, 389-402.

Zanin, Y.N., Zamirailova, A.G., Melenevskii, V.N., Davydov, D.Y., 1999. Two lithological and genetic types of black shales from the Bazhenov formation. Dokl. Akad. Nauk. 368, 946–999.

Zanin, Y.N., Zamirailova, A.G., Eder, V.G., Pisareva, G.M., 2003. Manganese carbonates in Upper Jurassic strata of the West Siberian Plate. Russian Geology and Geophysics. 44, 686–694.

Zanin, Y.N., Eder, V.G., Zamirailova, A.G., 2008. Composition and formation environments of the Upper Jurassic - Lower Cretaceous black shale Bazhenov formation (the central part of the west Siberian basin). Marine and Petroleum Geology. 25, 289–306.

Captions to Tables

Table 1. Mineral composition of some luminescent samples showing abundance of kaolin minerals in most samples and of mixed-layer I/S in sample P-1.

Table 2. Mineral composition of some non-luminescent lithotypes in Bazhenov Formation in well V-5 (Adapted from Shaldybin et al. (2017)).

Table 3. Trace element analysis (INAA and ICP-MS) for luminescent layers in ppm and for selected major (Na, Mg, Al, Ca, Fe and Ba) in %.

Table 4. Rock Eval results for Bazhenov suite samples in clayey-silty siliceous rocks above (A) and below (C) the luminescent argillite layer (B). (S1 is free HC in sample before analysis; S2 is volume of HC that formed during thermal pyrolysis. PI is Production Index S1/S2, Tmax is the temperature of maximum release of HC from cracking of kerogen, TOC is Total Organic Carbon, HI is Hydrogen Index and OI is Oxygen Index).

Table 5. Results of repeat element analyses for luminescent layer samples.

Minerals	Well					
	D-9	**K-4**	**E-7**	**P-1**	**V-5**	**S-2**
Quartz	2.1	1.8	2.7	1.9	1.5	2.6
Tridymite	1.0	1.2	0.0	1.0	1.3	1.5
Cristobalite	4.9	5.5	6.5	0.0	0.0	4.9
Potassium Feldspar	2.6	3.1	3.5	1.6	1.2	2.1
Plagioclase Feldspar	8.9	3.6	3.3	4.0	2.4	1.5
Kaolinite	53.9	64.0	61.7	29.1	70.6	78.6
Illite/Muscovite	6.2	5.3	5.7	8.2	3.6	1.5
Mixed-Layered Illite/Smectite	18.6	13.3	14.1	53.2	12.8	5.7
Calcite	0.0	1.1	1.2	0.0	0.0	0.0
Pyrite	1.8	1.1	1.3	1.0	5.0	1.6
Barite	0.0	0.0	0.0	0.0	1.6	0.0
Total, %	**100.0**	**100.0**	**100.0**	**100.0**	**100.0**	**100.0**

Table 1. Mineral composition of some luminescent samples showing abundance of kaolin minerals in most samples and of mixed-layer I/S in sample P-1.

Minerals	Sample N							
	6586	6588	6592	6596	6600	6601	6603	6604
Quartz	46	49	46	55	15	87	54	9
K Feldspar	0	0	0	0	0	2	1	3
Albite	8	9	8	9	1	1	7	1
Calcite	0	1	2	0	0	0	1	0
Dolomite	0	0	1	0	77	0	0	83
Illite + Illite/Smectite	39	29	33	24	0	4	24	0
Kaolinite	0	0	0	0	3	4	7	3
Chlorite	6	3	4	4	0	0	2	0
Pyrite	1	9	6	8	4	2	4	1
SUM	100	100	100	100	100	100	100	100

Table 2. Mineral composition of some non-luminescent lithotypes in Bazhenov Formation in well V-5 (Adapted from Shaldybin et al. (2017)).

Atomic No	Element	Well No											
		D-9 (Kaolinite rich)		K-4		V-5		D-9 (Illite-Smectite rich)		P-1		L-3	
		ICP-MS	INAA	ICP-MS	INAA	ICP-MS	INAA	ICP-MS	INAA	ICP-MS	INAA	ICP-MS	INAA
11	Na(%)	-	0.09	-	0.35	-	0.92	0,88	0.81	1,47	1.6	1,0	0.12
12	Mg(%)	0.12		1.10		0.90		0.36		0.58		0.82	
13	Al (%)	-		16.3		16.6		17.9		15.2		12.2	
20	Ca (%)	-	3.02	-	1.67	-	0.77		0.87		0.65		0.84
26	Fe (%)	0,97	0.96	1,62	1.53	1,09	1.07	1.21	0.35	1.27	1.41	1.02	1.29
56	Ba (%)	0.03	0.03	0.068	0.075	1.11	0.89	0.21	0.24	1.05	1.03	1.36	1.67
3	Li	16.0		110.0		6.9		133.0		25.0		9.0	
4	Be	0.16		<0.1		2.6		1.6		3.9		2.7	
15	P	120.0		730.0		1000.0		840.0		860.0		610.0	
21	Sc	<20.0	1.7	<20.0	7.45	<20.0	15.2	<20.0	4.1	<20.0	11.4	<20.0	14.1
22	Ti	480.0		2900.0		2600.0		2600.0		2700.0		1900.0	
23	V	67.0		1500.0		260.0		1901.0		1557.0		1310.0	
24	Cr	21.0	17.8	19.0	15.4	37.0	29.8	47.0	48.2	50.0	52.1	24.0	29.5
25	Mn	120.0		230.0		110.0		120.0		180.0		130.0	
27	Co	9.9	6.3	7.1	6.8	4.7	3.7	5.6	6.3	6.2	7.3	4.9	6.6
28	Ni	68.0		30.0		20.0		27.0		60.0		19.0	
29	Cu	33.0		43.0		100.0		41.0		110.0		64.0	
30	Zn	79.0	55.8	130.0	59.0	240.0	180.1	35.0	37.0	150.0	152.0	110.0	123.2
31	Ga	2.0		12.0		31.0		17.0		29.0		24.0	
32	Ge	0.6		0.87		0.34		0.11		0.14		0.19	
33	As	15.0	8.3	28.0	13.0	38.0	26.28	17.0	21.3	50.0	52.1	19.0	34.1
34	Se	13.0		16.0		22.0		11.0		25.0		33.0	
37	Rb	11.0	9.0	44.0	32.6	52.0	50.2	21.0	24.0	40.0	39.7	35.0	42.7
38	Sr	250.0	137.0	590.0	405.0	670.0	529.0	280.0	288.5	320.0	390.0	430.0	456.4
39	Y	3.7		11.0		21.0		3.8		8.2		16.6	
40	Zr	18.0		170.0		160.0		136.2		130.10		137.55	
41	Nb	1.40		3.20		4.30		1.28		1.94		2.79	
42	Mo	77.0		41.0		15.0		27.0		29.0		25.0	
48	Cd	1.5		0.64		3.0		0.54		2.9		2.2	
50	Sn	0.55		3.30		2.40		1.90		3.06		1.71	
51	Sb	2.2	1.01	2.2	1.08	5.4	3.18	4.4	3.66	9.1	8.08	3.9	4.05
55	Cs	0.64	0.51	5.4	4.9	5.1	4.35	2.0	2.22	3.0	3.37	3.7	5.35
57	La	2.8	4.05	21.0	25.1	68.0	69.56	16.0	20.97	31.0	39.2	25.0	45.9
58	Ce	5.0	9.6	50.0	50.15	130.0	121.3	35.89	37.0	59.39	59.25	54.1	68.38
59	Pr	0.67		5.2		13.0		3.5		5.7		4.9	
60	Nd	2.5	5.25	16.0	18.6	44.0	37.1	12.48	22.4	19.71	45.8	20.14	66.1
62	Sm	0.61	0,27	1.7	2.03	8.2	5.16	1.4	1.85	1.80	2.32	2.90	2.96
63	Eu	0.14	0.14	0.56	0.45	1.70	1.23	0.36	0.36	0.59	0.43	1.23	0.96
64	Gd	0.7		1.9		6.0		1.0		1.8		2.9	
65	Tb	0.12	0.09	0.35	<0.1	0.71	0.7	0.13	<0.05	0.20	0.28	0.44	0.36
66	Dy	0.6		1.9		3.8		0.89		1.35		3.11	
67	Ho	0.13		0.39		0.86		0.14		0.2		0.44	
68	Er	0.37		1.1		2.5		0.35		0.76		1.5	
70	Yb	0.46	0.50	0.88	1.26	2.2	2.16	0.56	<0.09	1.29	1.31	1.94	1.86
71	Lu	0.077	0.072	0.210	0.140	0.370	0.230	0.069	0.076	0.230	0.240	0.270	0.19
72	Hf	0.27	0.41	7.30	7.27	6.40	5.76	5.91	6.7	4.4.57	6.56	4.83	6.24
73	Ta	0.083	0.010	2.800	2.810	2.500	2.140	2.500	2.600	2.000	2.170	1.700	2.180
74	W	0.82		2.0		2.7		0.91		0.87		1.3	
81	Tl	0.61		0.40		0.44		0.61		1.3		0.50	
82	Pb	6.9		39.0		69.0		69.8		67.2		66.2	
83	Bi	0.05		2.3		2.4		2.1		1.6		1.5	
90	Th	0.92	0.92	79.00	70.80	76.00	57.20	74.00	77.00	63.00	55.90	54.00	31.90
92	U	14.0	11.2	40.0	32.7	67.0	51.6	20.5	18.6	28.8	26.7	80.0	77.6

Table 3. Trace element analysis (INAA and ICP-MS) for luminescent layers in ppm and for selected major (Na, Mg, Al, Ca, Fe and Ba) in %.

Well Name	Position of layer	Pyrolysis before extraction							Pyrolysis after extraction						
		S1, mg/g	S2, mg/g	PI= S1/ (S1+S2)	Tmax, °C	TOC, %	HI, mg HC/ g TOC	OI, mg CO_2/ g TOC	S1, mg/g	S2, mg/g	PI= S1/ (S1+S2)	Tmax, °C	TOC, %	HI, mg HC/ g TOC	OI, mg CO_2/ g TOC
K-4	A	5.89	110.09	0.05	429	15.54	708	1	0.18	94.38	0.00	429	13.82	683	4
K-4	B	0.46	1.07	0.30	418	0.27	396	0	0.04	0.62	0.07	425	0.25	248	24
K-4	C	6.12	115.17	0.05	428	15.90	724	1	0.24	106.86	0.00	427	14.88	718	2
E-7	A	8.00	123.14	0.06	433	16.96	726	0	0.15	108.37	0.00	433	15.54	697	2
E-7	B	0.66	1.16	0.36	412	0.52	223	2	0.03	0.54	0.06	423	0.23	235	35
E-7	C	7.33	137.01	0.05	432	18.60	737	0	0.17	122.95	0.00	431	16.87	729	0
M-10	A	2.97	68.54	0.04	438	9.97	687	2	0.14	64.01	0.00	436	9.82	652	3
M-10	B	0.54	5.39	0.09	432	1.08	499	10	0.04	4.30	0.01	432	1.04	413	10
M-10	C	2.96	41.71	0.07	440	6.74	619	1	0.12	38.84	0.00	438	6.36	611	3
D-9	A	9.13	95.13	0.09	438	15.40	618	0	0.09	79.98	0.00	438	13.32	600	0
D-9	B	0.66	1.45	0.31	371	0.54	269	0	0.04	0.62	0.06	419	0.29	214	0
D-9	C	5.78	108.91	0.05	440	17.10	637	0	0.14	96.69	0.00	437	15.60	620	2
V-5	A	5.08	52.59	0.09	439	8.49	619	0	0.06	37.41	0.00	439	6.93	540	3
V-5	B	0.80	1.70	0.32	419	1.14	149	7	0.07	0.69	0.09	424	0.96	72	14
V-5	C	2.99	63.09	0.05	439	10.13	623	0	0.06	50.30	0.00	437	8.92	564	1
S-2	A	7.67	38.79	0.17	437	7.81	497	0	0.07	24.37	0.00	436	5.81	419	3
S-2	B	0.85	4.46	0.16	431	0.98	455	0	0.05	2.26	0.02	432	0.63	359	2
S-2	C	8.56	59.28	0.13	440	10.34	573	0	0.10	45.83	0.00	439	8.27	554	0
P-1	A	2.45	19.88	0.11	444	5.40	368	0	0.08	14.01	0.01	442	4.65	301	0
P-1	B	0.73	2.64	0.22	407	0.70	377	0	0.03	1.05	0.03	424	0.47	223	0
P-1	C	2.28	19.36	0.11	440	5.02	386	0	0.05	11.63	0.00	444	3.90	298	0

Table 4. Rock Eval results for Bazhenov suite samples in clayey-silty siliceous rocks above (A) and below (C) the luminescent argillite layer (B). (S1 is free HC in sample before analysis; S2 is volume of HC that formed during thermal pyrolysis. PI is Production Index S1/S2, Tmax is

the temperature of maximum release of HC from cracking of kerogen, TOC is Total Organic Carbon, HI is Hydrogen Index and OI is Oxygen Index).

№	Well	Clay Type	Content			
			N, %	C, %	H, %	S, %
1	K-4	Kaolinite-rich	0,10	0,68	1,19	0,53
2			0,11	0,60	1,18	0,56
3	L-3	Kaolinite and Mixed-layer I/S	1,09	2,37	0,96	1,46
4			1,17	2,25	1,02	1,37
5	D-9	Mixed-layer I/S	1,21	0,94	1,02	1,19
6			1,45	0,83	1,09	1,21
7	P-1	Mixed-layer I/S rich	5,91	1,39	0,94	1,53
8			5,76	1,39	0,89	1,42
9	S-2	Kaolinite and Mixed-layer I/S	7,32	1,35	1,37	0,96
10			7,02	1,37	1,36	0,91
11	G-8	Kaolinite-rich	0,08	0,43	1,10	0,94
12			0,05	0,46	1,17	0,94
13	V-5	Mixed-layer I/S	1.69	0.60	1.30	1.20
14			2.49	0.57	1.27	1.24

Table 5. Results of repeat element analyses for luminescent layer samples.

Captions to Figures

Figure 1. Polished cross section of non-luminescing, organic-rich clayey-silty siliceous shale (dark upper layer) and organic-poor argillite (light lower layer) from the BSF.

Figure 2. Appearance of luminescent layers in argillite of the BSF in daylight and under UV radiation.

Figure 3. Well locations in the Bazhenov shale deposit (inset showing wider location in West Siberia and scale).

Figure 4. Optical micrographs showing the fabric of the luminescent layers of various thicknesses in the BSF in well D-9: A and C in orthogonal lamination, B – parallel lamination. Plane polarized light (left) and crossed polars (right). Notes: red circles - “volcanic debris” (or Glass); Q - quartz; OM – organic matter.

Figure 5. Fluorescence micrographs of argillite showing (a) discrete luminescent irregularly shaped volcanic ash particles and (b) junction between argillite and non-luminescent clayey-silty siliceous layer of BSF.

Figure 6. (a) SEM image of polished, carbon-coated thin sections of luminescent layers (in back-scattered electron mode) showing large blocky crystalline aggregates to left of field and a felted pseudo-fibrous texture to the right of the field, (b) EDS spectrum of blocky aggregates showing kaolinitic composition and (c) EDS spectrum of felted pseudo-fibrous material showing its aluminous composition but with significant K and Mg.

Figure 7. Bright field TEM image of the clay fraction of luminescent argillite from core P-1 showing thick aggregates of irregularly shaped platy particles, some with curled edges resembling fibres.

Figure 8. (a) Bright field TEM image of thick plate-like particle clearly showing a sub-structure of lath-like particles and (b) Selected area electron diffraction pattern from the edge of particle region shown in Fig. 8(a).

Fig. 9. (a) Selected area electron diffraction pattern from aggregated particle showing turbostratic prdering and (b) Selected area electron diffraction pattern from rolled up edge of platy particle showing (00l) and (hk0) reflections.

Figure 10. XRD patterns (CuKα radiation) of bulk samples of randomly oriented kaolinite-rich luminescent argillite. Values of d-spacing are given in angstroms. Mineral identification: I/S - illite-smectite mixed layered minerals, K - kaolinite, Q – quartz, F – feldspars, P - pyrite, M - marcasite, C – calcite

Figure 11. XRD patterns of the bulk sample (a) and clay fraction (b) of oriented illite-rich argillite (sample P-1) in air-dried (blue), glycol solvated (red) and heated at 550°C (yellow). Values of d-spacing are given in angstroms. Mineral identification: I/S - illite-smectite mixed layered minerals, K - kaolinite, Q – quartz, F – feldspars, P - pyrite, M - marcasite, C - calcite

Figure 12. IR spectra of (a) a luminescent argillite sample from D-9 well; (b) well-crystallized kaolinite from Georgia, USA and (c) dickite from Anglesey, North Wales.

Figure 13. Characterisation of (a) oil-generating potential and (b) maturity and type of organic matter (OM) of A, B and C layers of the Bazhenov Shale Formation. (A and C - clayey-silty siliceous shales; B - luminescent argillites).

Figure 14. (a) SEM image of pseudo-fibrous felted clay from a luminescent layer and kaolinite clay and (b) Element map of the same showing that the K and Mg ions are located in the pseudo-fibrous aggregates surrounding kaolinitic clay.

Figure 15. Diagram showing dependence of S2 (volume of HC formed during pyrolysis) vs Total Organic Carbon. Note: x-intercept goes through 0.5% TOC.

Figure 16. Photographs of a luminescent layer sample in day light (top) and under UV light (bottom) after heating at increasing temperatures. Note that the luminescent effect disappears at just above 400ºC.

Figure 17. FTIR spectra of the Bazhenov shale sample from a luminescent layer following heating to temperatures of 400, 500, 700, 800 and 900ºC. Note: the band at 1432cm^{-1} disappears after heating to 500°C.

Figure 18. Plot of luminescent layer samples on the magmatic discriminant diagram of Winchester and Floyd (1977) (Data from Table 3).

1984), which are found to promote the luminescence of kaolinite clay. The distribution of organic compounds in source rocks and related crude oils have shown large and systematic variation due to fractionation effects associated with the primary and secondary migration processes (Yamamoto, 1992; Li et al., 1995). Bennett and Love (2000) studied samples of the Kimmeridge Clay Formation and identified a significant range of nitrogen-containing organic compounds and concluded that this indicates the formation of nitrogen compounds at a relatively early stage of diagenesis. This possibly suggests that similar nitrogen compounds may occur in the luminescent layers of the BSF which is close to the stratigraphic equivalent of the Kimmeridge Clay.

5.2. Origin of the luminescent layers

The evidence outlined above indicates that some specific luminescent layers in inter-bedded argillites of the BSF can be described as meta-tuffites as meta-tuffites and are analogous to K-bentonite (kaolinitic K-bentonite) and are composed primarily of volcanic ash material, but with a significant contribution of silt-sized minerals of terrigenous origin that are typical of the BSF as a whole. The clay mineralogy of these luminescent layers is undoubtedly almost exclusively authigenic in origin as shown by the extraordinary morphology of the kaolinite/dickite and ordered mixed-layer I/S clays which is clearly incompatible with normal detrital sedimentation. As for the conditions under which the kaolin minerals formed, although Ehrenberg et al. (1993) suggested that kaolinite transformed to dickite at about 3km depth at temperatures of 120-130ºC in Mesozoic sandstones of the North Sea, later studies by Beaufort et al. (1998) and Lanson et al. (2002) suggest that a progressive transformation to dickite can occur at lower temperatures and more shallow depths as a result of kinetic and other factors.

Comment [ШМ114]: Added according to recommendations of Rev#2

Captions to Figures

Fig. 1. Polished cross section of non-luminescing, organic-rich clayey-silty siliceous shale (dark upper layer) and organic-poor argillite (light lower layer) from the BSF.

Fig. 2. Appearance of luminescent layers in argillite of the BSF in daylight and under UV radiation.

Fig. 3. Well locations in the Bazhenov shale deposit (inset showing wider location in West Siberia and scale).

Fig. 4. Optical micrographs showing the fabric of the luminescent layers of various thicknesses in the BSF in well D-9: A and C in orthogonal lamination, B – parallel lamination. Plane polarized light (left) and crossed polars (right). Notes: red circles - “volcanic debris” (or Glass); Q - quartz; OM – organic matter.

Fig. 5. Fluorescence micrographs of argillite showing (a) discrete luminescent irregularly shaped volcanic ash particles and (b) junction between argillite and non-luminescent clayey-silty siliceous layer of BSF.

Fig. 6. (a) SEM image of polished, carbon-coated thin sections of luminescent layers (in back-scattered electron mode) showing large blocky crystalline aggregates to left of field and a felted pseudo-fibrous texture to the right of the field, (b) EDS spectrum of blocky aggregates showing kaolinitic composition and (c) EDS spectrum of felted pseudo-fibrous material showing its aluminous composition but with significant K and Mg.

Fig. 7. Bright field TEM image of the clay fraction of luminescent argillite from core P-1 showing thick aggregates of irregularly shaped platy particles, some with curled edges resembling fibres.

Fig. 8. (a) Bright field TEM image of thick plate-like particle clearly showing a sub-structure of lath-like particles and (b) Selected area electron diffraction pattern from the edge of particle region shown in Fig. 8(a).

Fig. 9. (a) Selected area electron diffraction pattern from aggregated particle showing turbostratic prdering and (b) Selected area electron diffraction pattern from rolled up edge of platy particle showing (00l) and (hk0) reflections.

Figure 10. XRD patterns (CuKα radiation) of bulk samples of randomly oriented kaolinite-rich luminescent argillite. Values of d-spacing are given in angstroms. Mineral identification: I/S - illite-smectite mixed layered minerals, K - kaolinite, Q – quartz, F – feldspars, P - pyrite, M - marcasite, C - calcite

Figure 11. XRD patterns of the bulk sample (a) and clay fraction (b) of oriented illite-rich argillite (sample P-1) in air-dried (blue), glycol solvated (red) and heated at 550°C (yellow). Values of d-spacing are given in angstroms. Mineral identification: I/S - illite-smectite mixed layered minerals, K - kaolinite, Q – quartz, F – feldspars, P - pyrite, M - marcasite, C – calcite

Fig. 12. IR spectra of (a) a luminescent argillite sample from D-9 well; (b) well-crystallized kaolinite from Georgia, USA and (c) dickite from Anglesey, North Wales.

Fig. 13. Characterisation of (a) oil-generating potential and (b) maturity and type of organic matter (OM) of A, B and C layers of the Bazhenov Shale Formation. (A and C - clayey-silty siliceous shales; B - luminescent argillites).

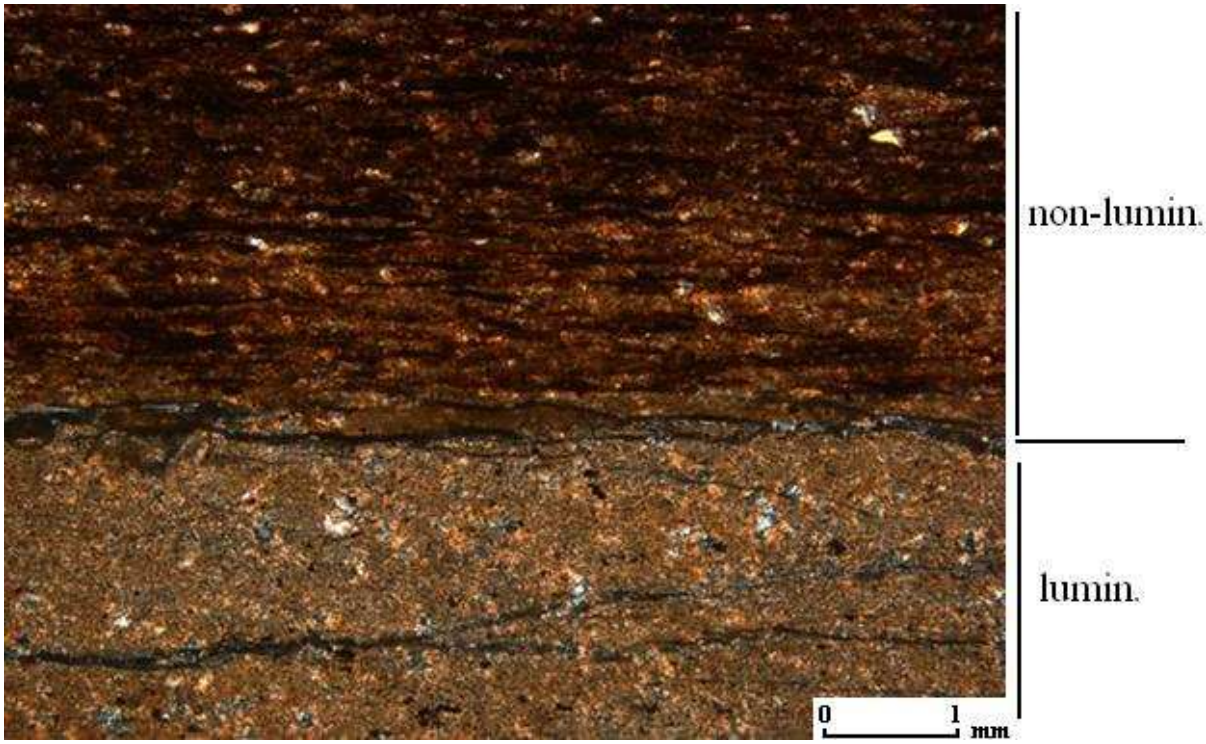

Fig. 1. Polished cross section of non-luminescing, organic-rich clayey-silty siliceous shale (dark upper layer) and organic-poor argillite (light lower layer) from the BSF.

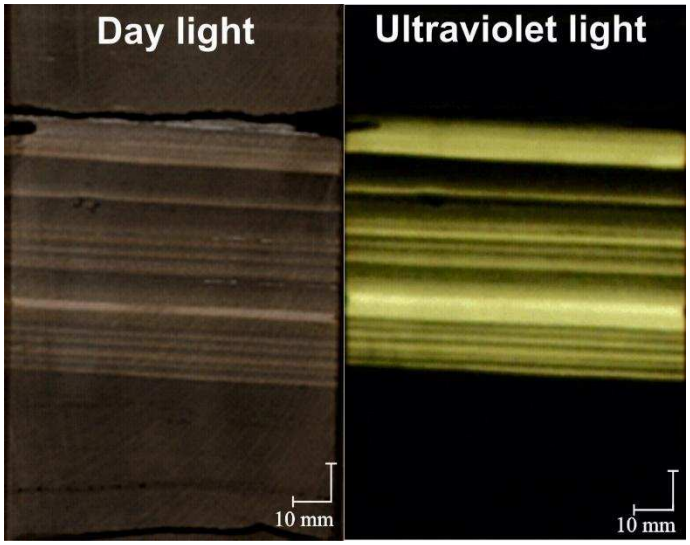

Fig. 2. Appearance of luminescent layers in argillite of the BSF in daylight and under UV radiation.

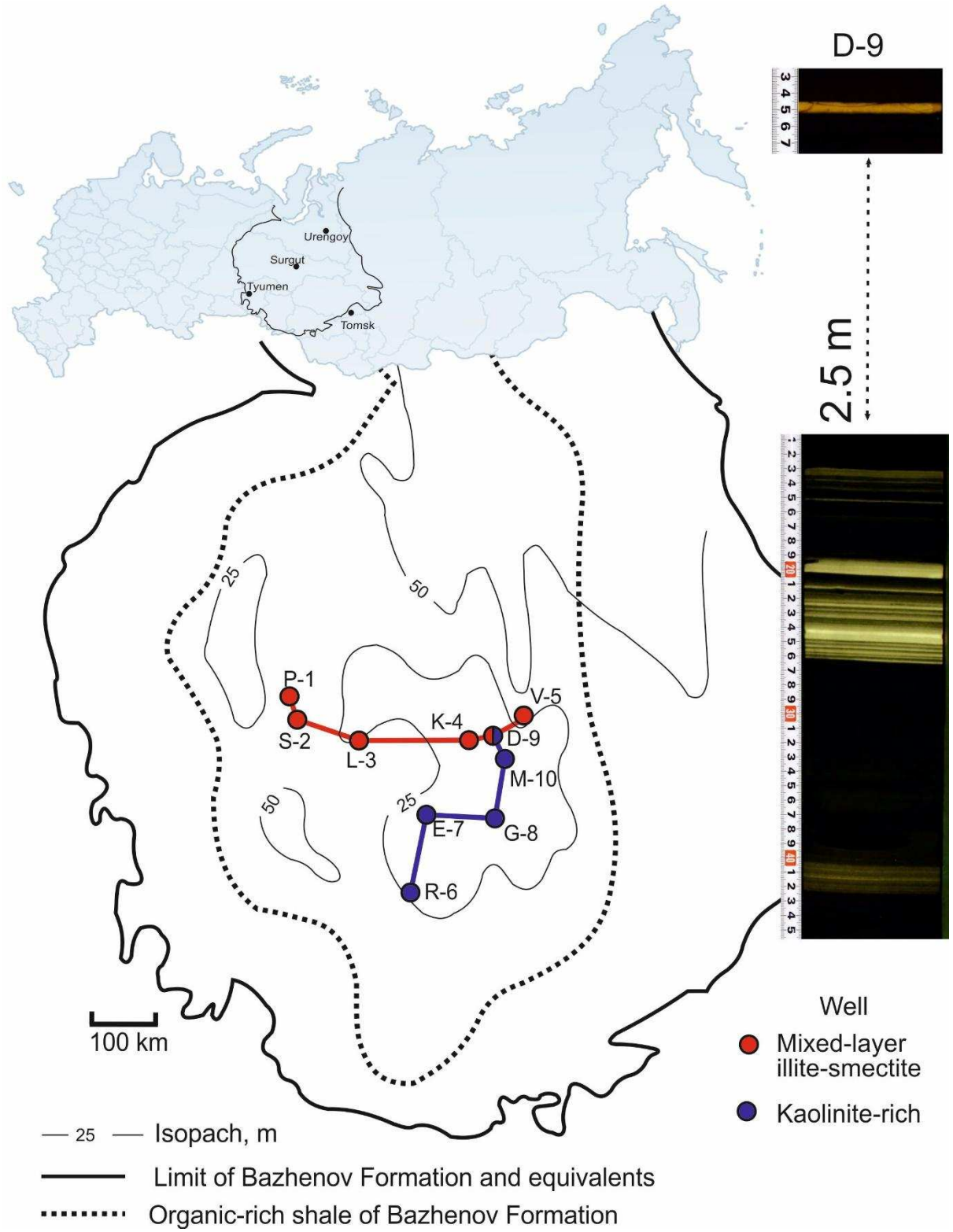

Fig. 3. Well locations in the Bazhenov shale deposit (inset showing wider location in West Siberia and scale).

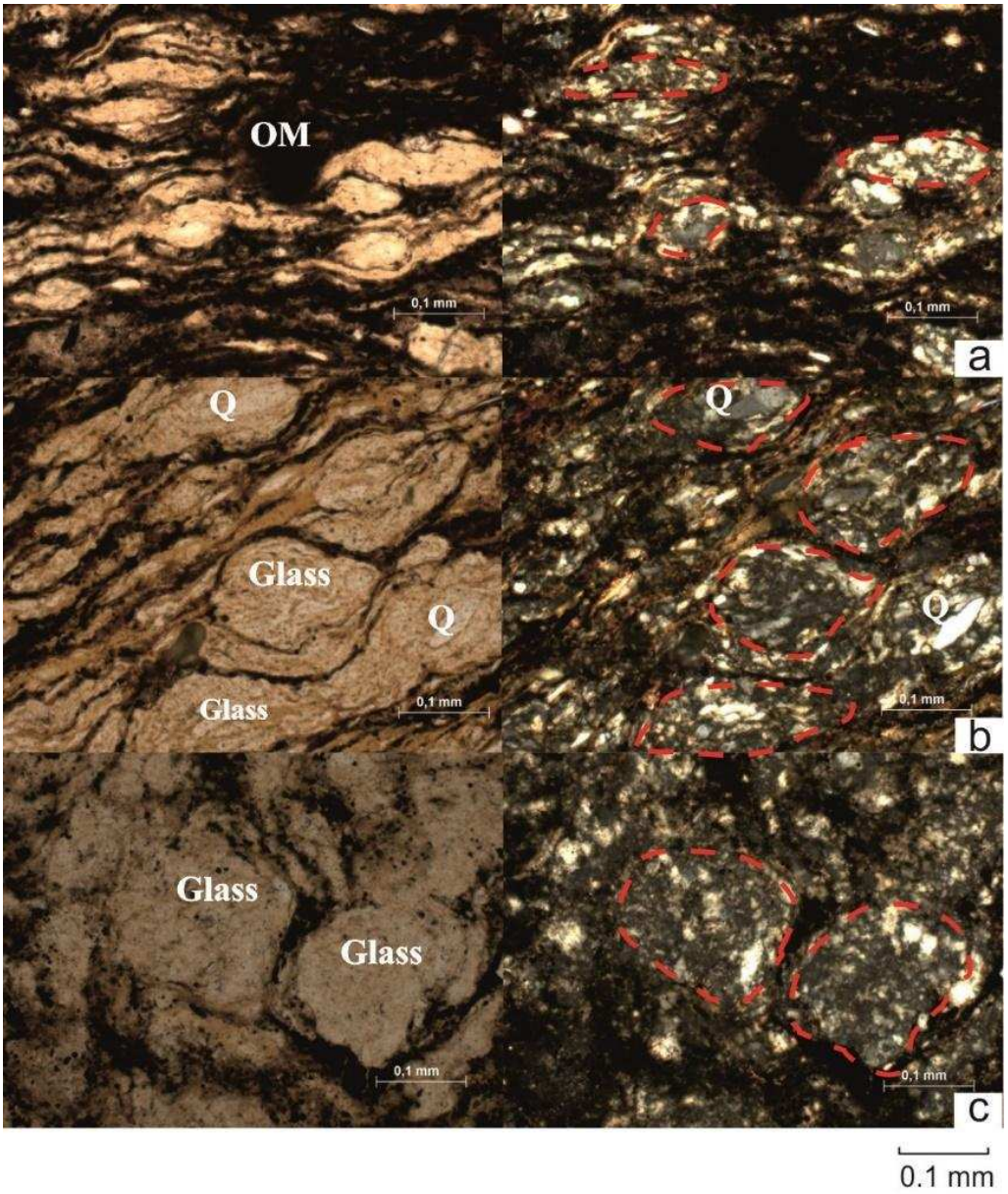

Fig. 4. Optical micrographs showing the fabric of the luminescent layers of various thicknesses in the BSF in well D-9: A and C in orthogonal lamination, B – parallel lamination. Plane polarized light (left) and crossed polars (right). Notes: red circles - “volcanic debris” (or Glass); Q - quartz; OM – organic matter.

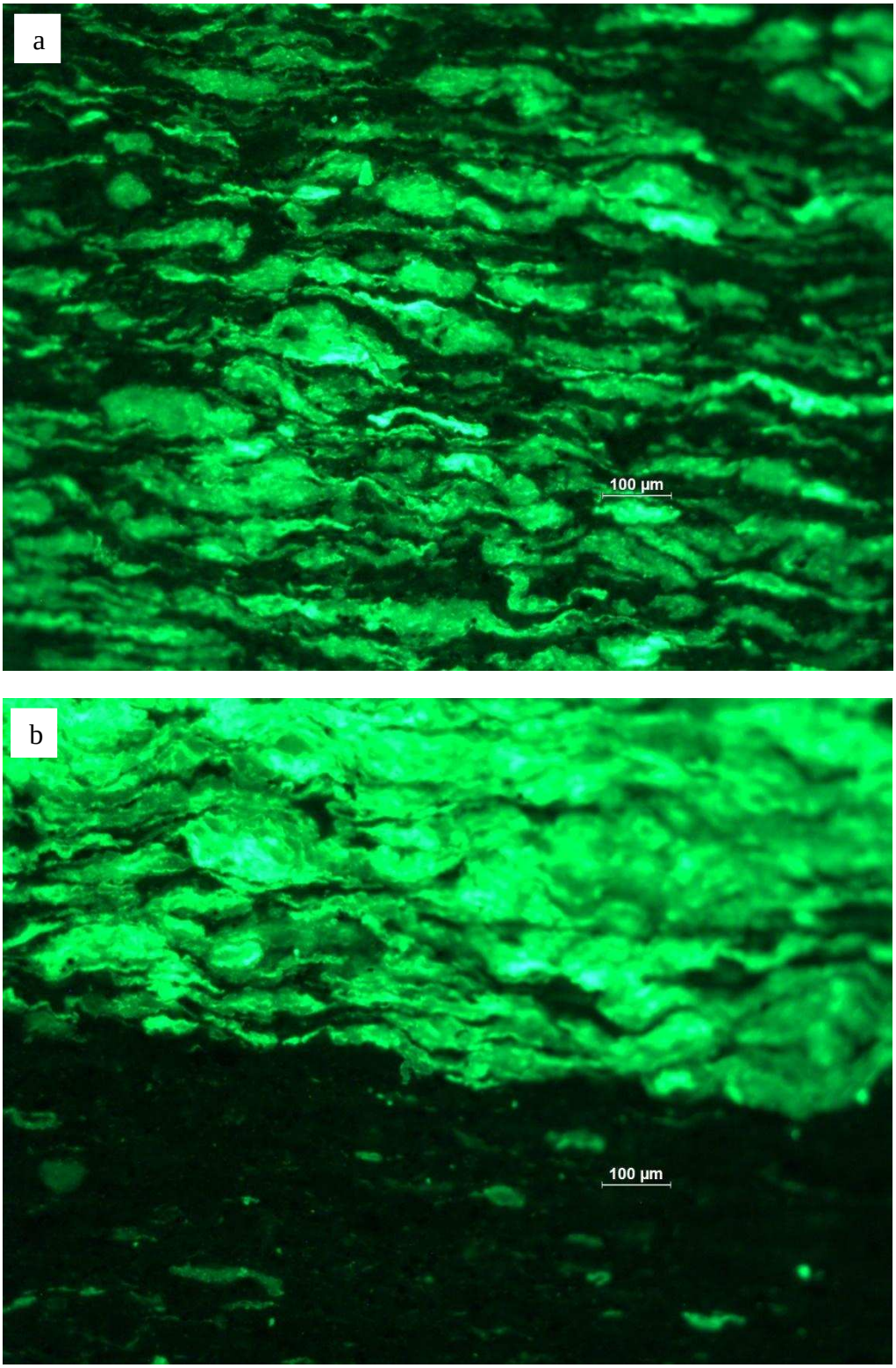

Fig. 5. Fluorescence micrographs of argillite showing (a) discrete luminescent irregularly shaped volcanic ash particles and (b) junction between argillite and non-luminescent clayey-silty siliceous layer of BSF.

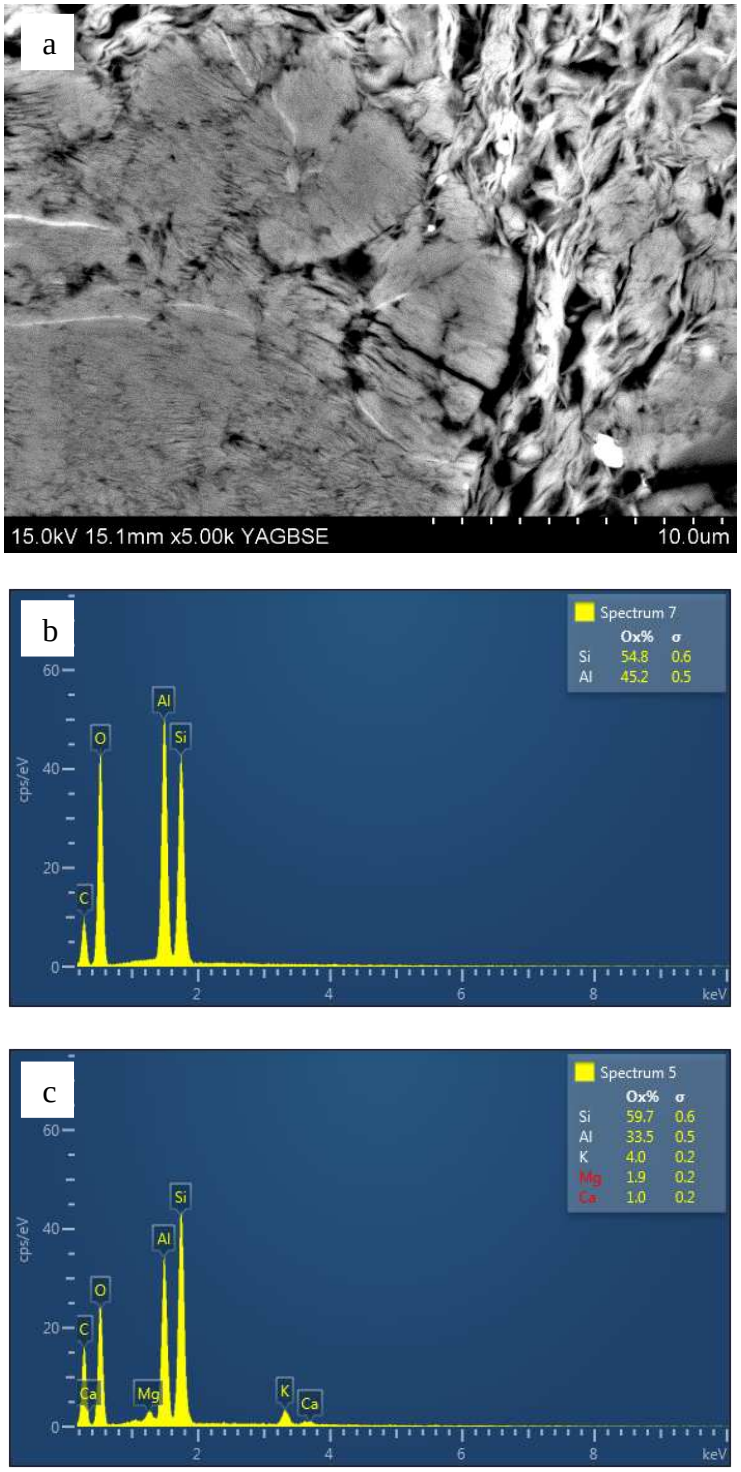

Fig. 6. (a) SEM image of polished, carbon-coated thin sections of luminescent layers (in back-scattered electron mode) showing large blocky crystalline aggregates to left of field and a felted pseudo-fibrous texture to the right of the field, (b) EDS spectrum of blocky aggregates showing kaolinitic composition and (c) EDS spectrum of felted pseudo-fibrous material showing its aluminous composition but with significant K and Mg.

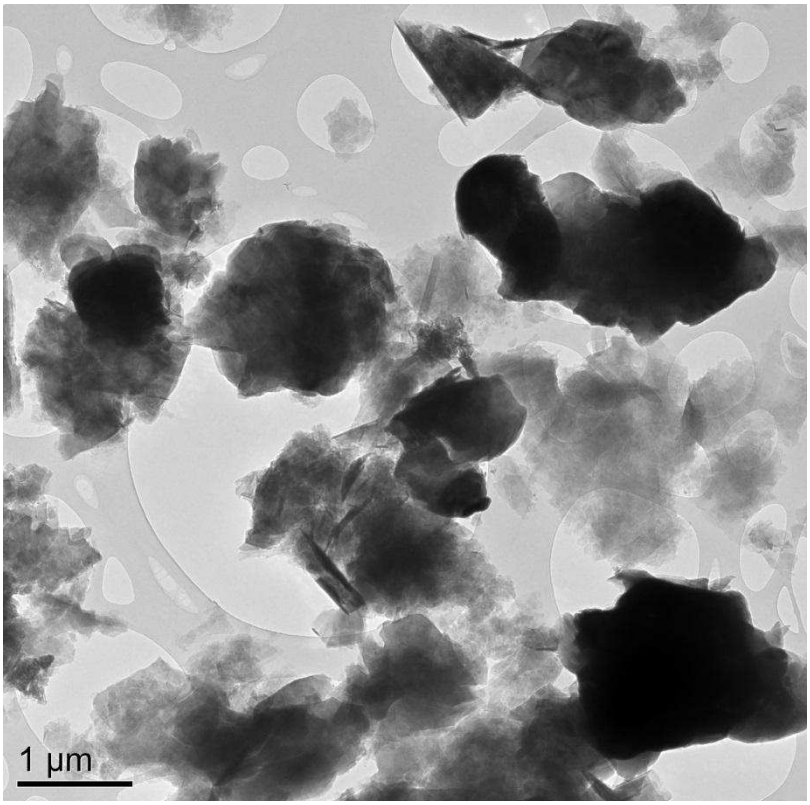

Fig. 7. Bright field TEM image of the clay fraction of luminescent argillite from core P-1 showing thick aggregates of irregularly shaped platy particles, some with curled edges resembling fibres.

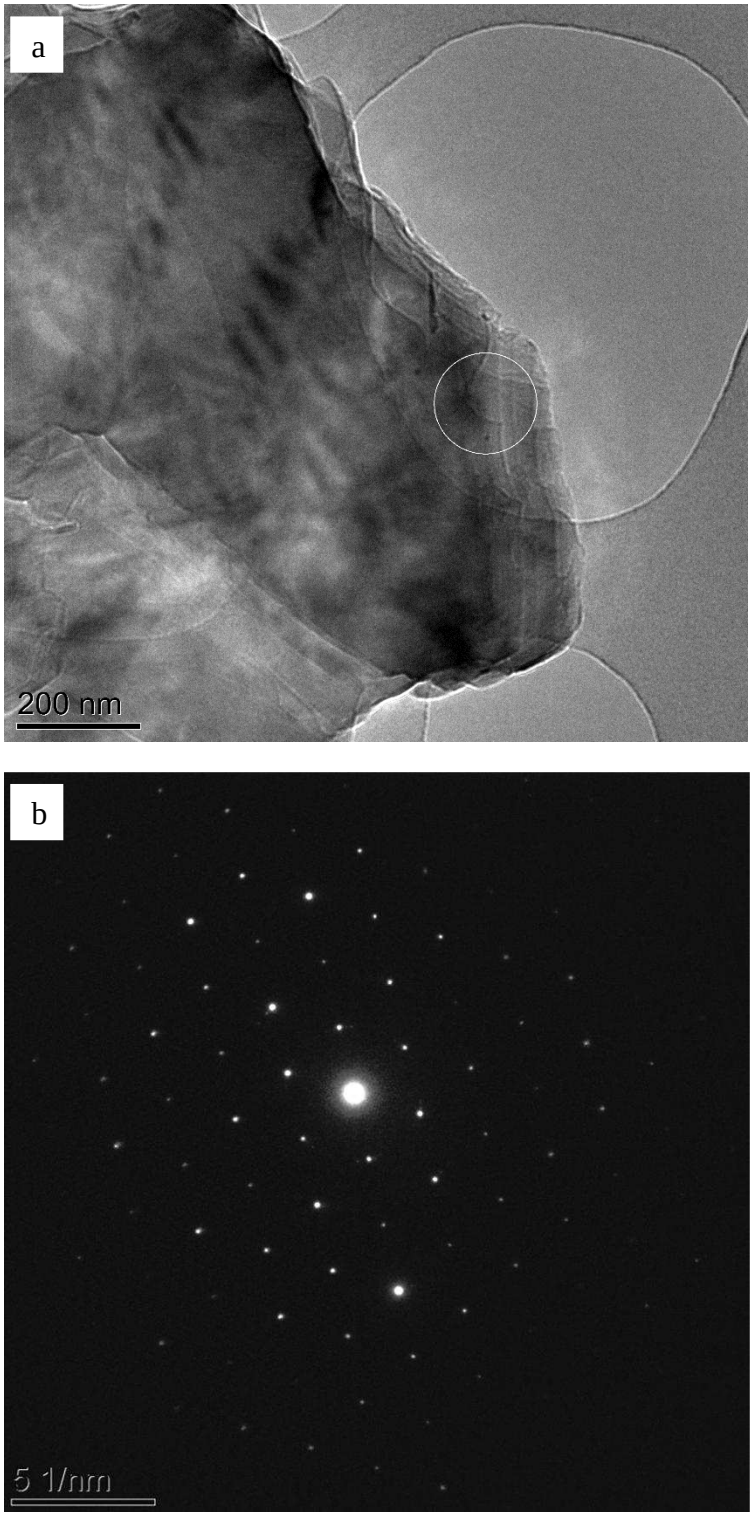

Fig. 8. (a) Bright field TEM image of thick plate-like particle clearly showing a sub-structure of lath-like particles and (b) Selected area electron diffraction pattern from the edge of particle region shown in Fig. 8(a).

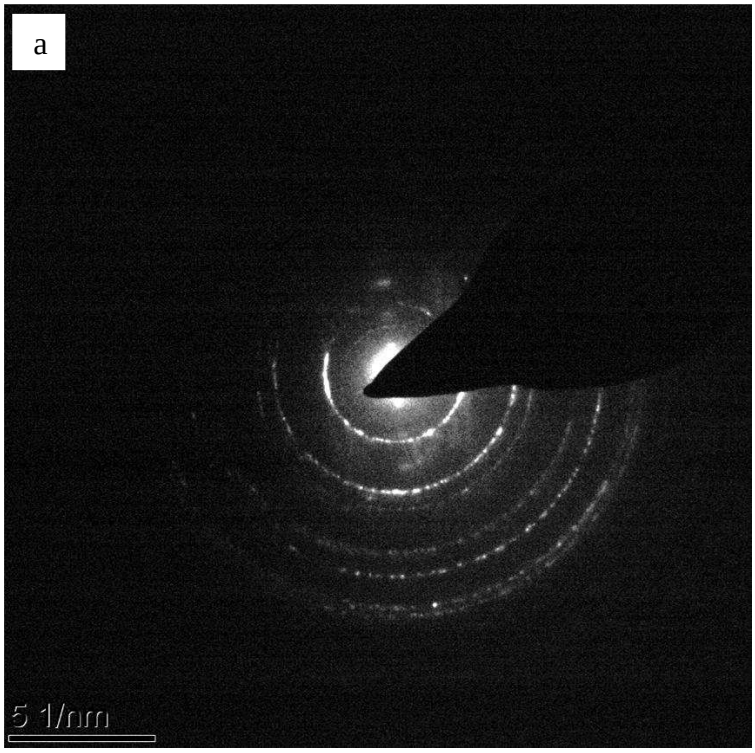

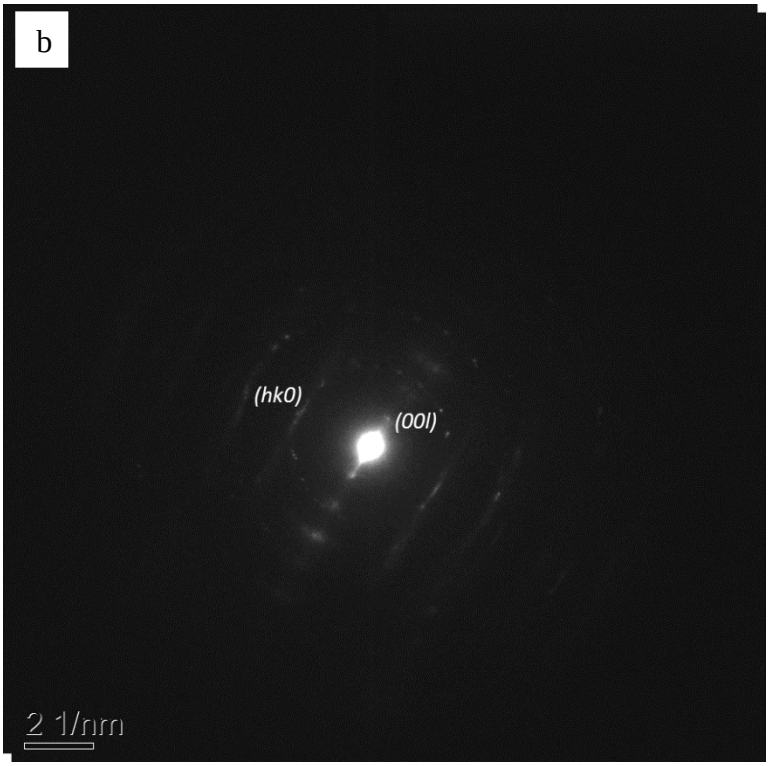

Fig. 9. (a) Selected area electron diffraction pattern from aggregated particle showing turbostratic prdering and (b) Selected area electron diffraction pattern from rolled up edge of platy particle showing (00l) and (hk0) reflections.

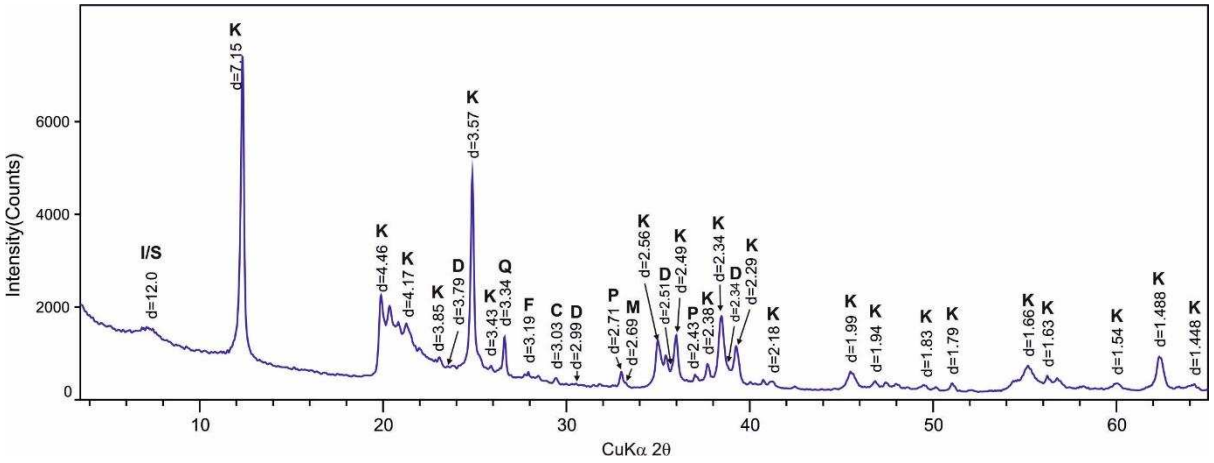

Figure 10. XRD patterns (CuKα radiation) of bulk samples of randomly oriented kaolinite-rich luminescent argillite. Values of d-spacing are given in angstroms. Mineral identification: I/S - illite-smectite mixed layered minerals, K - kaolinite, Q – quartz, F – feldspars, P - pyrite, M - marcasite, C - calcite

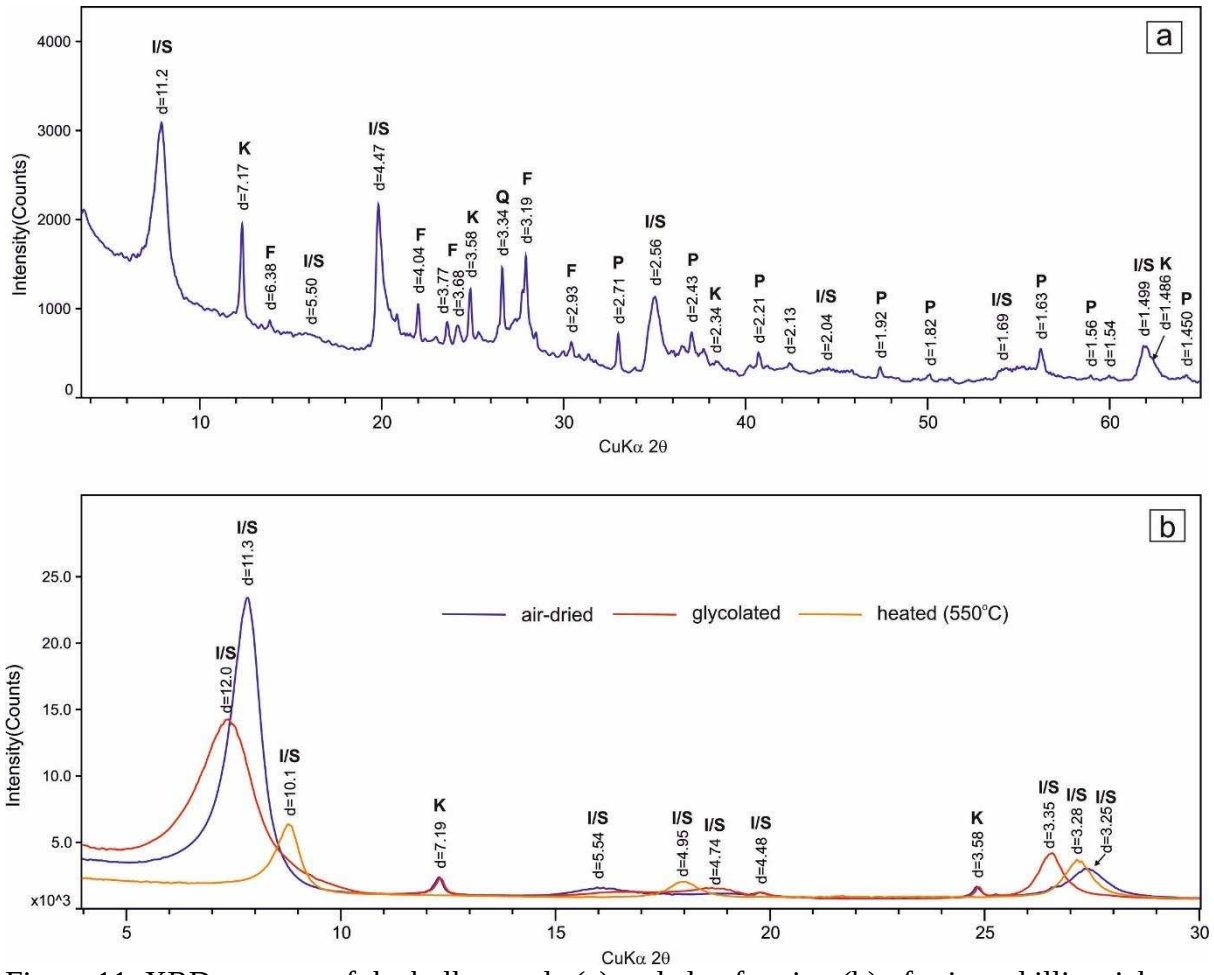

Figure 11. XRD patterns of the bulk sample (a) and clay fraction (b) of oriented illite-rich argillite (sample P-1) in air-dried (blue), glycol solvated (red) and heated at 550°C (yellow). Values of d-spacing are given in angstroms. Mineral identification: I/S - illite-smectite mixed layered minerals, K - kaolinite, Q – quartz, F – feldspars, P - pyrite, M - marcasite, C – calcite

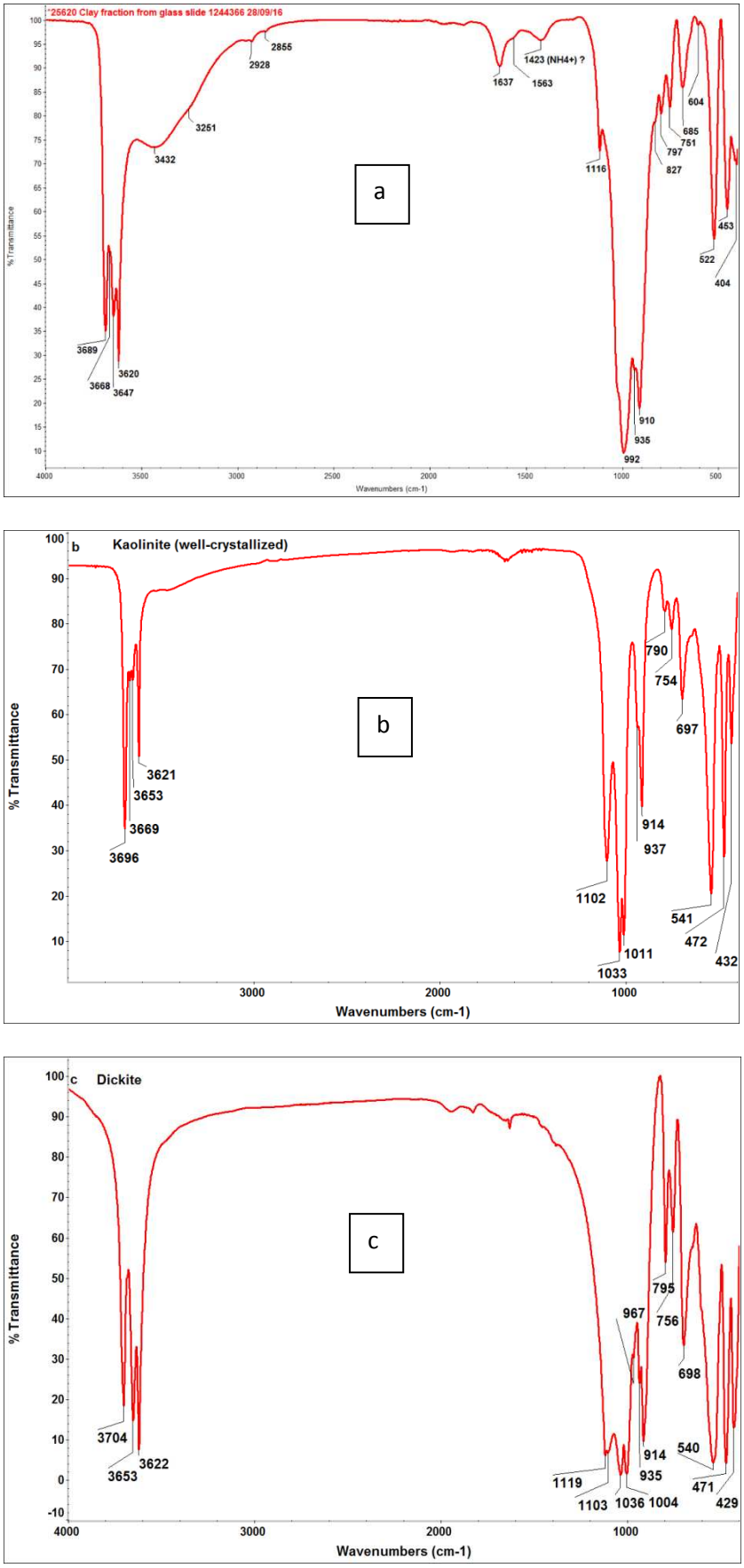

Fig. 12. IR spectra of (a) a luminescent argillite sample from D-9 well; (b) well-crystallized kaolinite from Georgia, USA and (c) dickite from Anglesey, North Wales.

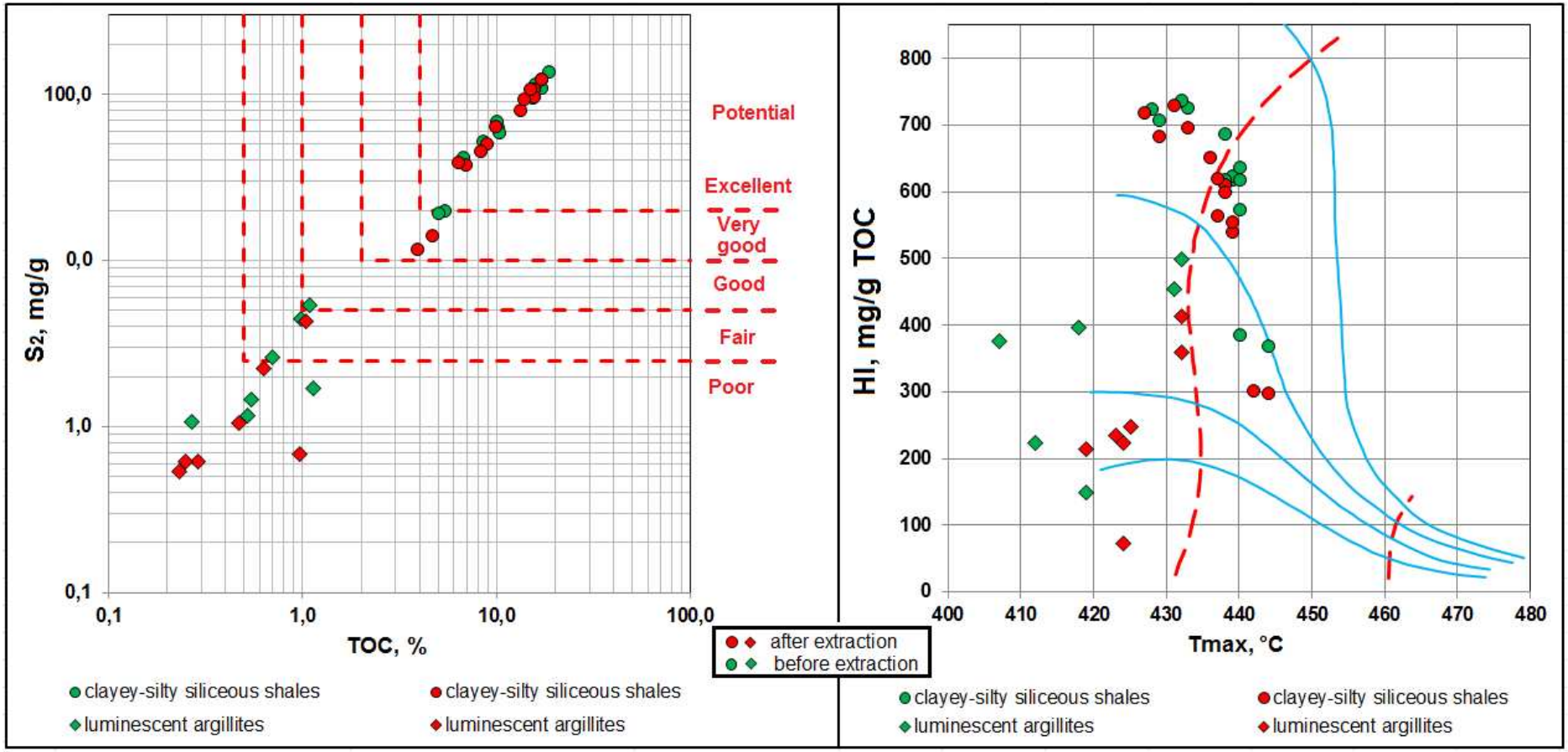

Fig. 13. Characterisation of (a) oil-generating potential and (b) maturity and type of organic matter (OM) of A, B and C layers of the Bazhenov Shale Formation. (A and C - clayey-silty siliceous shales; B - luminescent argillites).

a

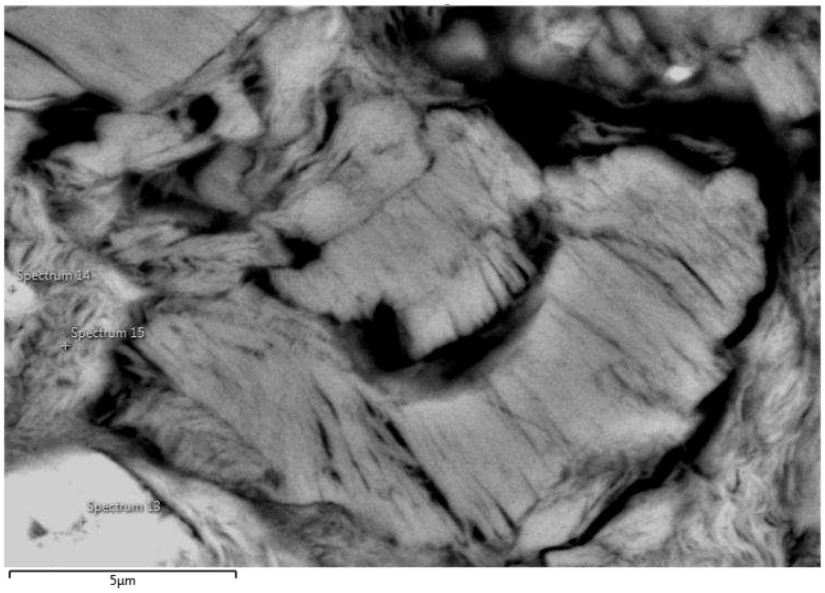

b

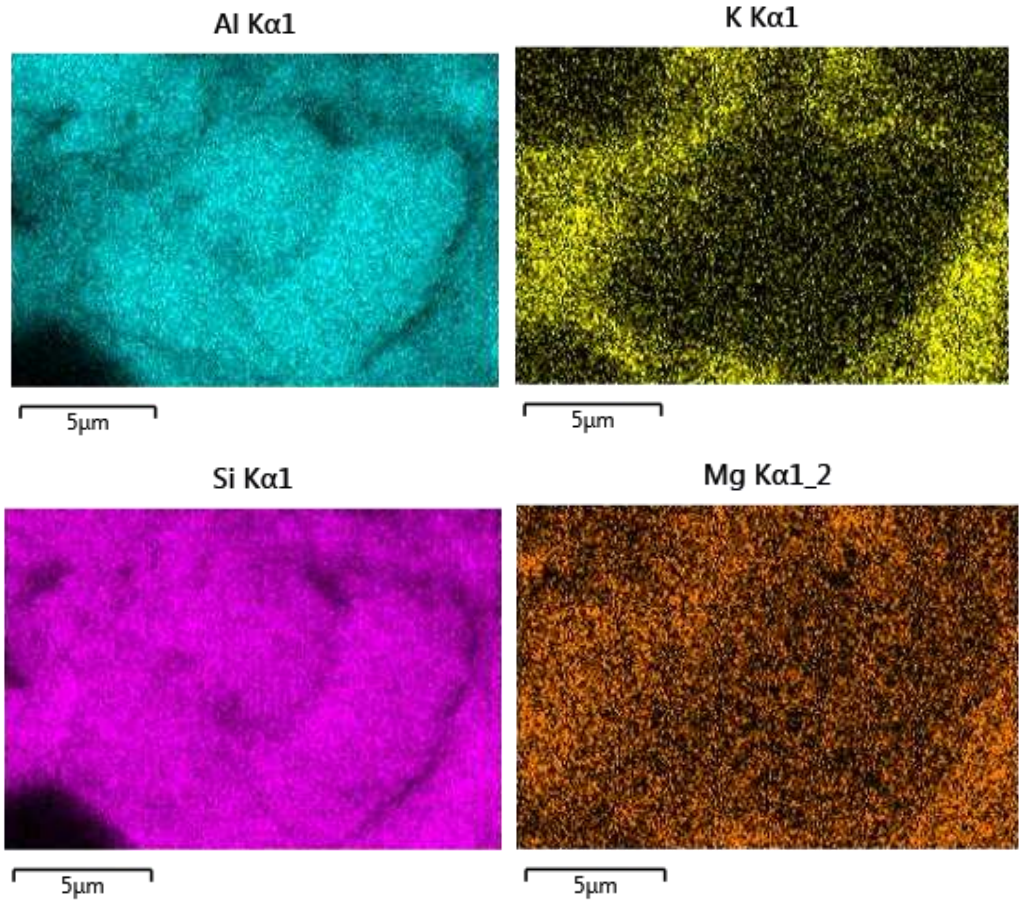

Fig. 14. (a) SEM image of pseudo-fibrous felted clay from a luminescent layer and kaolinite clay and (b) Element map of the same showing that the K and Mg ions are located in the pseudo-fibrous aggregates surrounding kaolinitic clay.

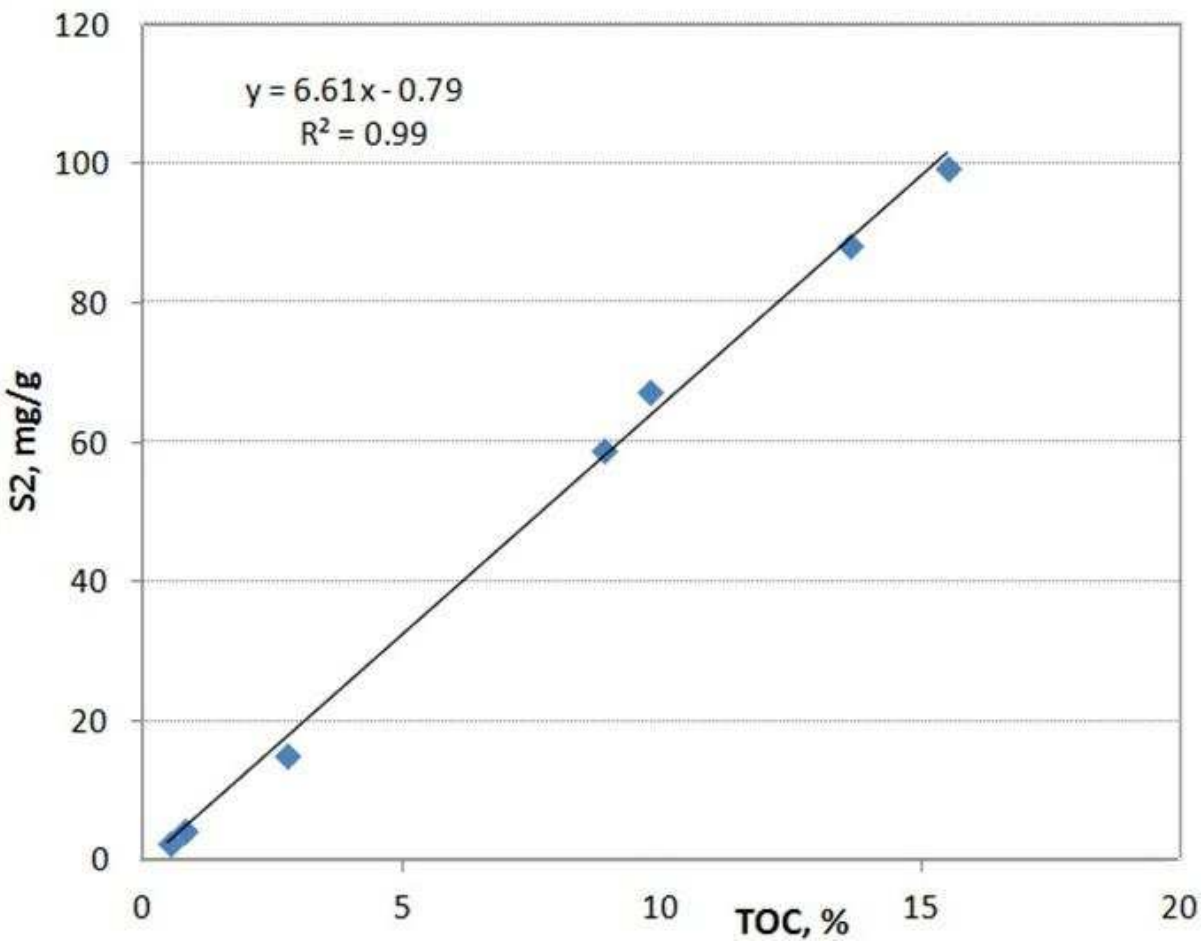

Fig. 15. Diagram showing dependence of S2 (volume of HC formed during pyrolysis) vs Total Organic Carbon. Note: x-intercept goes through 0.5% TOC.

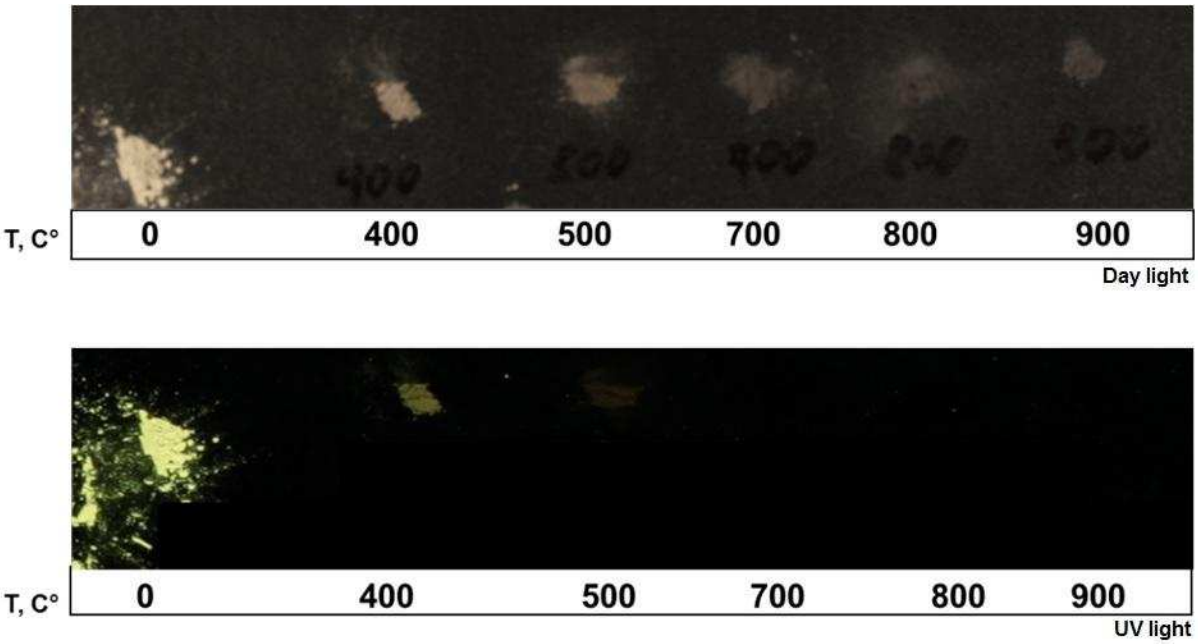

Fig. 16. Photographs of a luminescent layer sample in day light (top) and under UV light (bottom) after heating at increasing temperatures. Note that the luminescent effect disappears at just above 400ºC.

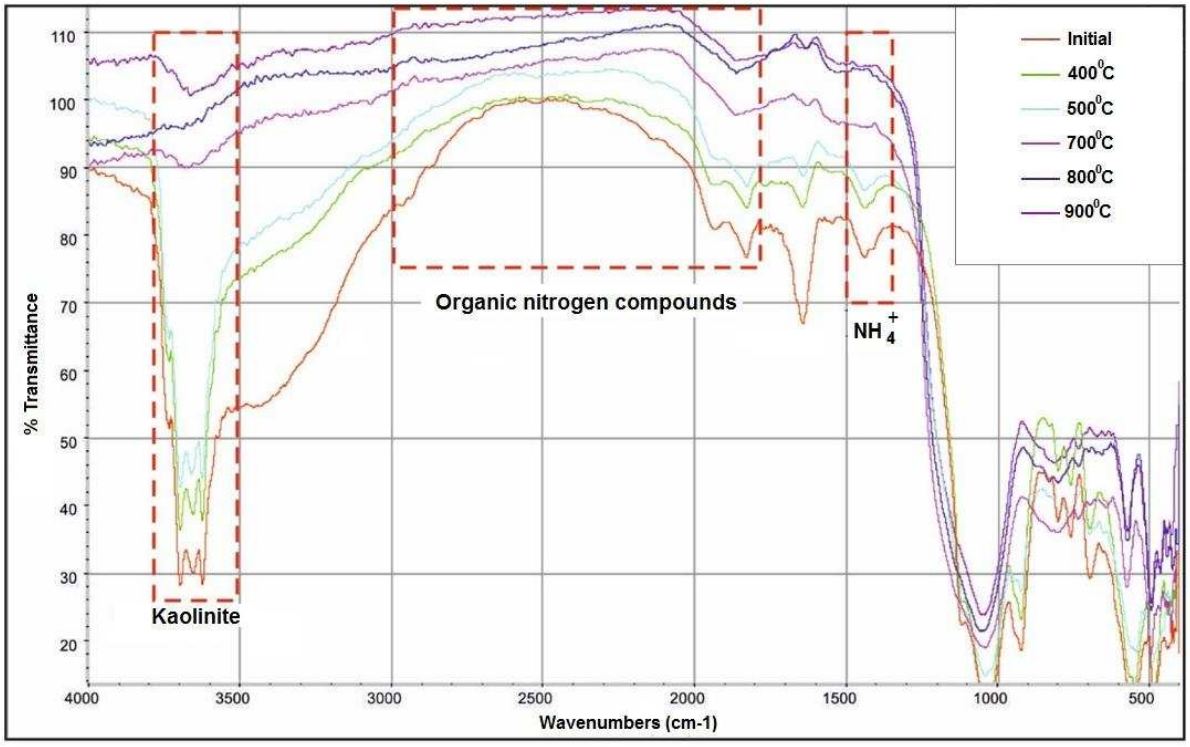

Fig. 17. FTIR spectra of the Bazhenov sample from a luminescent layer sample following heating to temperatures of 400, 500, 700, 800 and 900ºC. Note: the band at 1432cm^{-1} disappears after heating to 500°C.

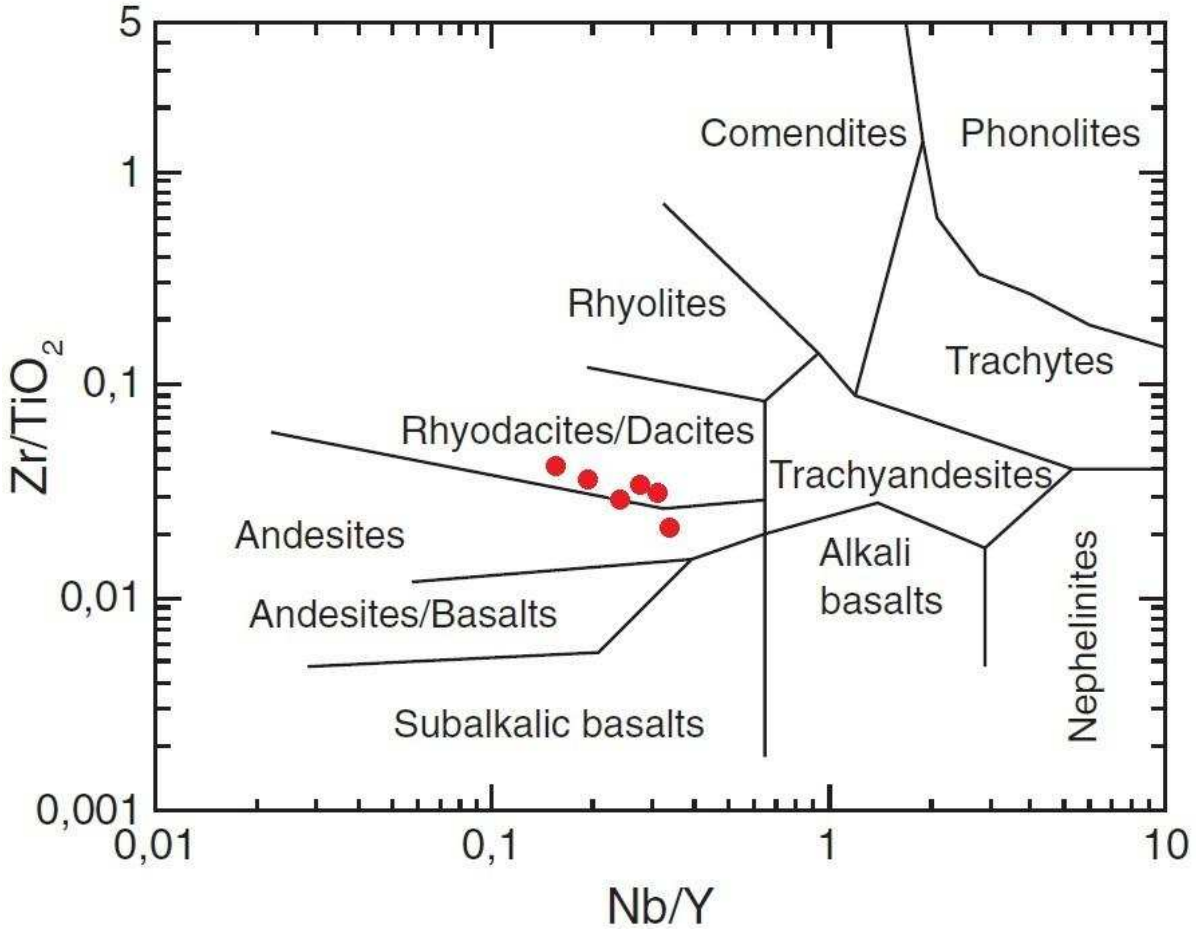

Fig. 18. Plot of luminescent layer samples on the magmatic discriminant diagram of Winchester and Floyd (1977) (Data from Table 3).